Analyses of cell wall synthesis in *Clostridioides difficile* reveal a diversification in cell division mechanisms in endospore-forming bacteria

Shailab Shrestha[1,2], Najwa Taib[3,4], Simonetta Gribaldo[3], Aimee Shen[1,*]

[1]Department of Molecular Biology and Microbiology, Tufts University School of Medicine, Boston, MA, USA. [2]Program in Molecular Microbiology, Tufts University Graduate School of Biomedical Sciences, Boston, MA, USA. [3]Institut Pasteur, Université de Paris, Unit Evolutionary Biology of the Microbial Cell, Paris, France. [4]Institut Pasteur, Université Paris Cité, Bioinformatics and Biostatistics Hub, F-75015 Paris, France.

*Address correspondence to
Aimee Shen, aimee.shen@tufts.edu
Phone number: (617)636-3792

Author Contributions

S.S. and A.S. conceived the study. S.S. performed and analyzed experiments. S.S. and N.T. conducted bioinformatic analyses. A.S. supervised the study. S.S. and A.S. wrote the manuscript with input from N.T. and S.G. All authors reviewed and approved the manuscript.

Abstract

Current models of bacterial cell division assume that the core synthases of the multiprotein divisome complex, FtsW-FtsI, are the primary drivers of septal peptidoglycan (PG) synthesis. These enzymes are typically encoded in the highly conserved division and cell wall (*dcw*) cluster and are considered to be universally essential for cell division. Here, we combine bioinformatics analyses with functional characterization in the pathogen *Clostridioides difficile* to show that *dcw*-encoded PG synthases have undergone a surprising specialization in the sole endospore-forming phylum, Firmicutes, to fulfill sporulation-specific roles. We describe a novel role for these enzymes in synthesizing septal PG during the sporulation-specific mode of cell division in *C. difficile*. Although these enzymes are directly regulated by canonical divisome components during this process, *dcw*-encoded PG synthases and their divisome regulators are unexpectedly dispensable for cell division during normal growth. Instead, *C. difficile* uses its sole bifunctional class A penicillin-binding protein (aPBP) to drive cell division, revealing a previously unreported role for this class of PG synthases as the core divisome enzyme. Collectively, our findings reveal how the emergence of endosporulation in the Firmicutes phylum was a key driver for the functional repurposing of an otherwise universally conserved cellular process such as cell division. Moreover, they indicate that *C. difficile,* and likely other clostridia, assemble a divisome that differs markedly from previously studied bacteria, thus representing an attractive, unique target for therapeutic purposes.

Introduction

Synthesis of cell wall peptidoglycan (PG) is essential for growth and division in most bacteria. The extra-cytoplasmic assembly of PG results from two sequential enzymatic reactions: a transglycosylation reaction that polymerizes the PG precursor Lipid II into glycan strands and a transpeptidation reaction that crosslinks these glycan strands together to form a protective meshwork (Egan et al., 2020).

Our understanding of this critical process has been transformed by the recent discovery that SEDS (shape, elongation, division, and sporulation) family proteins function as PG glycosyltransferases in complex with cognate class B penicillin-binding protein (bPBP) transpeptidases to synthesize PG (Meeske et al., 2016; Cho et al., 2016; Emami et al., 2017; Taguchi et al., 2019). Current models posit that specific SEDS-bPBP pairs function as the core PG synthases driving either cell elongation or division in rod-shaped bacteria (Emami et al., 2017; Leclercq et al., 2017; Meeske et al., 2016; Reichmann et al., 2019; Sjodt et al., 2020; Taguchi et al., 2019). These specialized pairs of SEDS-bPBPs associate with specific multiprotein assemblies to mediate either cell elongation or cell division: lateral growth is

32 typically driven by the SEDS-bPBP pair, RodA-MrdA, as a part of the elongasome, while septum
33 formation is mediated by the SEDS-bPBP pair, FtsW-FtsI, as a part of the divisome.
34 Prior to the discovery of SEDS glycosyltransferases, class A penicillin-binding proteins (aPBPs)
35 were the only known PG synthases with glycosyltransferase activity. Unlike monofunctional bPBP
36 transpeptidases, aPBPs are bifunctional enzymes that harbor both glycosyltransferase and transpeptidase
37 activities and they were presumed to be the primary PG synthases driving cell elongation and division
38 (Straume et al., 2021). However, recent evidence suggests that aPBPs often play non-essential, peripheral
39 roles during these processes, consistent with their absence from the genomes of many obligate
40 intracellular bacteria (Cho et al., 2016; Dion et al., 2019; Straume et al., 2020; Vigouroux et al., 2020).
41 Indeed, aPBPs can function independently of the divisome and elongasome and appear to mainly modify
42 and repair PG synthesized by SEDS-bPBP enzymes (Atwal et al., 2021; Straume et al., 2020, 2021).
43 Notably, these models of bacterial PG synthesis primarily derive from studies in *Escherichia coli*
44 and *Bacillus subtilis*, but studies in organisms with different cell morphologies and mechanisms of growth
45 have variably supported and challenged these general models. For instance, all Actinobacteria and some
46 Proteobacteria follow a polar growth model where cell growth is driven by PG synthesis at cell poles. In
47 these organisms, cell elongation is largely mediated by aPBP activity (Joyce et al., 2012; Kieser et al.,
48 2015; Sher et al., 2021; Williams et al., 2021). Given the diversity of mechanisms involved in bacterial
49 PG synthesis and the importance of studying these processes in diverse bacteria, the functional
50 characterization of major PG synthases in different bacteria is an area of significant interest.
51 Although diverse mechanisms of cell elongation have been described in bacteria, cell division
52 mechanisms appear to be broadly conserved. Divisome-guided septal PG synthesis is mediated by the
53 essential SEDS-bPBP enzyme pair, FtsW-FtsI, which is considered to be universally conserved in all
54 bacteria (Taguchi et al., 2019). Genes encoding these enzymes are typically located within the division
55 and cell wall (*dcw*) cluster (Megrian et al., 2022), which contains numerous genes involved in PG
56 synthesis and cell division. Recent phylogenetic analyses have revealed that the *dcw* locus is widely
57 conserved across almost all bacterial phyla and likely originated in the Last Common Bacterial Ancestor
58 billions of years ago (Megrian et al., 2022).
59 Despite this extreme conservation, the *dcw* cluster SEDS gene in the model endospore-forming
60 bacterium *Bacillus subtilis* does not encode FtsW, but rather SpoVE, a sporulation-specific SEDS
61 glycosyltransferase that is critical for endospore formation (Piggot & Coote, 1976; Ikeda et al., 1989;
62 Henriques et al., 1992). In *B. subtilis*, SpoVE forms a complex with the sporulation-specific bPBP
63 SpoVD to synthesize a thick protective PG layer known as the cortex during sporulation (Daniel et al.,
64 1994; Fay et al., 2010; Yanouri et al., 1993). Notably, *B. subtilis* is a member of the Firmicutes phylum,
65 which is the only bacterial phyla to have evolved endospore formation. Since the formation of highly

resistant, mature spores depends on a series of peptidoglycan transformations unique to endospore-forming bacteria, we hypothesized that the Firmicutes would exhibit greater variation in the composition and function of bPBP and SEDS genes in their *dcw* loci. Here, we analyzed the distribution of PG synthase-encoding genes in the *dcw* loci of Firmicutes organisms and analyzed their function in the medically important clostridial pathogen, *Clostridioides difficile*. These analyses revealed a previously unappreciated diversification in the mechanisms by which *C. difficile,* and likely other clostridia, mediates cell division during vegetative growth and endospore formation.

Results

Diversity of *dcw*-encoded PG synthesizing enzymes based on sporulation potential

Firmicutes are unique among bacteria in forming endospores. While the last common ancestor of the Firmicutes is thought to have been an endospore former, the ability to sporulate has been independently lost among members of this phylum (Garcia et al., 2021) (Fig. 1, Supplementary Fig. 1, Supplementary Tables 2, 3). To analyze the distribution of genes encoding SEDS glycosyltransferases and bPBPs in the *dcw* cluster of both spore-forming and non-spore-forming Firmicutes organisms, we constructed a custom database consisting of 494 Firmicutes genomes representative of the six major classes described in this phylum. Next, we inferred the organism's ability to form endospores by determining the presence of *spo0A* and *spoIIE* in all Firmicutes genomes. These genes are both part of a core genomic signature of sporulating bacteria (Galperin et al., 2022) and encode key regulators required for initiating and committing cells to sporulation, respectively (Ferrari et al., 1985; Margolis et al., 1991), so their co-occurrence strongly suggests that a given species is a spore former. We searched for SEDS and bPBP homologs in all Firmicutes genomes and identified genes encoding SEDS and bPBP enzymes in the *dcw* cluster based on their synteny with other genes of the *dcw* cluster (*mraW*, *mraY*, *ftsZ*, *mraZ,* and *murCDEF*). We also identified a pair of SEDS and bPBP homologs, RodA and MrdA, respectively, involved in cell elongation and located in a different locus. Finally, we identified SEDS homologs encoded adjacent to the gene encoding pyruvate carboxylase, PycA (Fig. 1, Supplementary Fig. 1, 2, Supplementary Table 2)**.**

In agreement with what has been described in *Bacillus subtilis* (Yanouri et al., 1993), sporulating taxa from Bacilli encode two homologs of bPBPs in the *dcw* cluster, which most probably correspond to the canonical cell division PG synthesizing enzyme, FtsI, and the sporulation-specific PG synthesizing enzymes, SpoVD (Fig. 1). Non-sporulating Bacilli only have a single bPBP gene in their *dcw* clusters, suggesting that *spoVD* was lost from this locus coincident with the loss of sporulation; the remaining bPBP gene in the *dcw* locus presumably encodes *ftsI*. In contrast, sporulating Bacilli encode only a single SEDS glycosyltransferase gene in their *dcw* loci. This gene likely encodes SpoVE based on functional

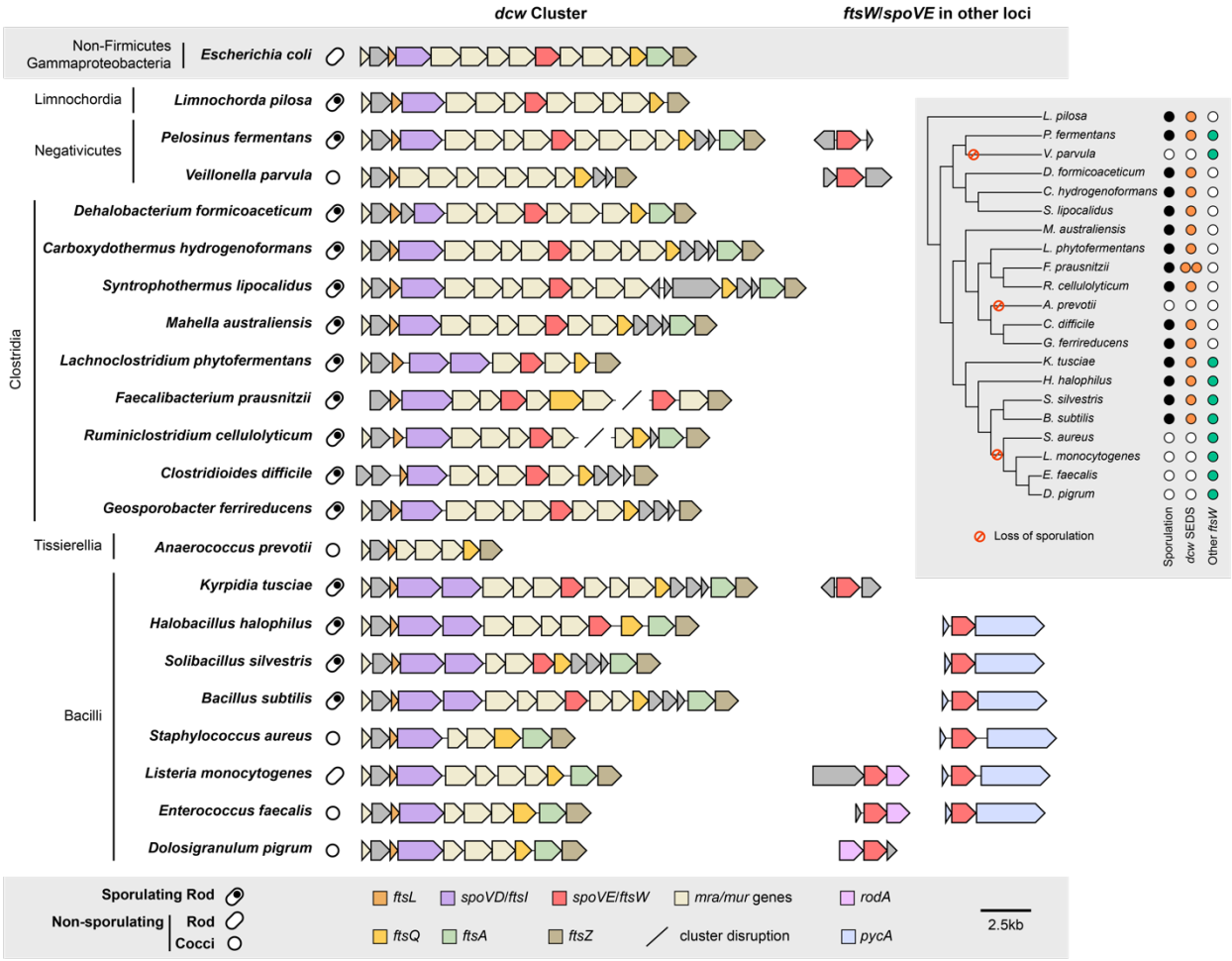

Fig. 1 | Comparison of *dcw* cluster composition and occurrence of SEDS family proteins across diverse Firmicutes species. The ability to form spores was inferred by the presence of broadly conserved sporulation-specific genes *spo0A* and *spoIIE* in the genome (Galperin et al., 2022). SEDS homologs that cluster with the cell elongation-associated RodA encoding genes were excluded from the analyses (Supplementary Fig. 2). For genome accession numbers, coordinates, and taxonomy information, see Supplementary Table 1. The inset tree shows phylogenetic relationships and the presence or absence of sporulation genes (*spo0A* and *spoIIE*), *dcw*-encoded SEDS gene(s), and *ftsW* orthologs encoded outside the dcw cluster for each organism. The colored circles highlight the presence (black) and loss of sporulation (red) genes, as well as the presence of *ftsW*/*spoVE* within (orange) and outside (green) the *dcw* cluster. For analyses of the full dataset, see Supplementary Fig. 1.

analyses in *B. subtilis* (Piggot & Coote, 1976; Ikeda et al., 1989; Henriques et al., 1992) and our finding that non-sporulating Bacilli lack SEDS genes altogether from their *dcw* loci (Fig. 1). Thus, SEDS genes appear to have been lost from the *dcw* cluster coincident with the loss of sporulation. Notably, all Bacilli carry a SEDS glycosyltransferase gene outside of the *dcw* cluster (usually adjacent to *pycA* (Fig. 1)) that codes for a canonical cell division FtsW ortholog; the essential function of this conserved gene has been validated in several members of the Bacilli (Perez et al., 2019; Reichmann et al., 2019; Rismondo et al., 2019; Taguchi et al., 2019), suggesting that *dcw*-encoded PG synthesizing enzymes became specialized to functional exclusively during spore formation.

115 The same arrangement between sporulating and non-sporulating species can be observed in the
116 Class Negativicutes and Limnochordia (Fig. 1), suggesting that the homologs present in their *dcw* clusters
117 of sporulating members of these classes also encode SpoVE and SpoVD. Together, these analyses reveal
118 that the presence of SEDS and bPBP genes in the *dcw* cluster is highly correlated with sporulation
119 (Supplementary Table 3), and that the genes present in the *dcw* cluster of sporulating Firmicutes code for
120 SpoVE and SpoVD, respectively, rather than the canonical cell division proteins FtsW and FtsI.
121 Exceptions are represented by some members of the Clostridia, Tissierellia, and Erysipelotrichia, which
122 display a mixed pattern (Supplementary Fig. 1, Supplementary Table 2). Surprisingly, Clostridia do not
123 appear to have any extra copy of division-specific SEDS and bPBP in their *dcw* cluster or elsewhere in
124 the genomes, suggesting they completely lack the canonical cell division pair FtsW-FtsI. Therefore, we
125 sought to define the functions of dcw-encoded SEDS and bPBP genes of the genetically tractable
126 clostridial species *C. difficile*.

127 **The *dcw*-encoded SEDS-bPBP pair in *C. difficile* participates in septal PG synthesis during spore**
128 **formation but not vegetative growth**

129 To this end, we determined the effect of deleting the *dcw*-encoded SEDS and bPBP genes, *spoVE*
130 and *spoVD*, on *C. difficile* growth and sporulation. Consistent with the results of a prior transposon screen
131 indicating that *spoVE* and *spoVD* are non-essential for growth (Dembek et al., 2015), we were able to
132 create single deletion strains lacking *spoVD* or *spoVE*. These strains did not exhibit growth or
133 morphological defects during vegetative growth (Fig. 2a, b), indicating that *C. difficile* SpoVD and
134 SpoVE are not involved in vegetative cell division. Consistent with prior work (Alabdali et al., 2021;
135 Srikhanta et al., 2019), the *C. difficile* Δ*spoVD* strain failed to make heat-resistant spores (Supplementary
136 Fig. 3) or synthesize a cortex layer based on transmission electron microscopy (TEM) analyses
137 (Supplementary Fig. 4). Similar phenotypes were observed for the Δ*spoVE* strain, indicating that *C.*
138 *difficile* SpoVD and SpoVE share similar functions with their orthologs in *B. subtilis* in regulating cortex
139 synthesis (Daniel et al., 1994; Fay et al., 2010; Henriques et al., 1992; Yanouri et al., 1993). Importantly,
140 the sporulation defect of these mutants could be fully complemented from a chromosomal ectopic locus
141 (Supplementary Fig. 3).

142 However, in contrast with *B. subtilis*, we observed that *C. difficile* Δ*spoVD* and Δ*spoVE* mutants
143 appeared to sporulate at lower levels than WT, with few cells exhibiting visible signs of sporulation
144 during phase-contrast microscopy analyses (Supplementary Fig. S3). To investigate whether SpoVD and
145 SpoVE affect sporulation processes earlier than cortex synthesis, we evaluated the ability of
146 Δ*spoVD* and Δ*spoVE* cells to progress through the different morphological stages of sporulation using

147 cytological profiling (Nonejuie et al., 2013; Pogliano et al., 1999). These analyses revealed that most
148 visibly sporulating Δ*spoVD* and Δ*spoVE* cells were stalled at the asymmetric division stage, with a

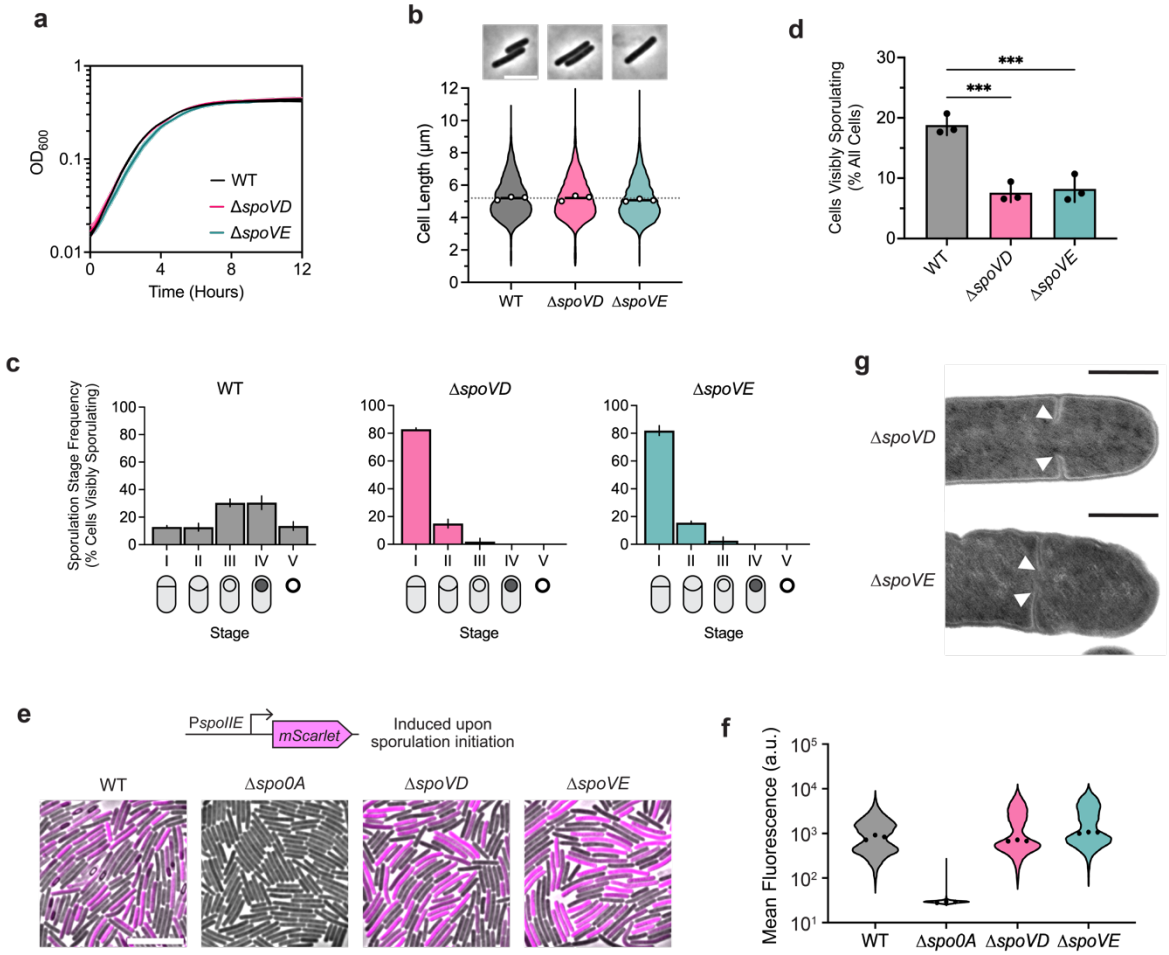

149 **Fig. 2 | Sporulation-specific PG synthases, SpoVD and SpoVE, are important for asymmetric but not**
150 **vegetative division. a,** Growth profiles of *C. difficile* wildtype (WT), Δ*spoVD,* and Δ*spoVE* strains in BHIS. Data
151 are from a single experiment; mean and standard deviation curves are plotted from three biological replicates. **b,**
152 Violin plots showing cell length distributions and representative micrographs of WT, Δ*spoVD,* and Δ*spoVE* cells
153 sampled from BHIS cultures during exponential growth (OD_{600} ~0.5). White circles indicate means from each
154 replicate, black lines indicate average means, and the dotted line indicates the WT average mean for comparison
155 across strains. Data from three biological replicates; >1,500 cells per sample. Scale bar, 5 μm. **c, d,** Cytological
156 profiling of WT, Δ*spoVD,* and Δ*spoVE* cells sampled from sporulation-inducing 70:30 plates after 18-20 hours of
157 growth. Cells were assigned to five distinct stages based on their membrane (FM4-64) and DNA (Hoechst) staining
158 and their phase-contrast morphological phenotypes. For representative micrographs and stage assignment
159 information, see Supplementary Fig. 3. Bars indicate means; error bars indicate standard deviation. ***p<0.001;
160 statistical significance was determined using ordinary one-way ANOVA with Dunnett's test. Data from three
161 independent experiments; >1,000 total cells and >100 visibly sporulating cells per sample. **e,** Representative merged
162 phase-contrast and fluorescence micrographs visualizing P_{spoIIE}::*mScarlet* transcriptional reporters in sporulating
163 WT, Δ*spoVD,* and Δ*spoVE* cells sampled from 70:30 plates after 14-16 hours of growth. P_{spoIIE} is induced
164 immediately upon sporulation initiation. The Δ*spo0A* strain was used as a negative control because it does not
165 initiate sporulation. Scale bar, 10 μm. **f,** Violin plots showing quantified mean fluorescence intensities. Black dots
166 represent median values from each replicate. Data from three independent experiments; >3,000 cells per sample. **g,**
167 Transmission electron micrographs of Δ*spoVD* and Δ*spoVE* sporulating cells that fail to complete septum formation
168 24 hrs after sporulation induction (white arrows). Scale bars, 500 nm.

169 relatively small proportion completing engulfment compared to wild-type (WT) cells (Fig. 2c,
170 Supplementary Fig. 5). Strikingly, the overall proportions of Δ*spoVD* and Δ*spoVE* cells exhibiting
171 morphological signs of sporulation, i.e., cells that have completed or progressed beyond asymmetric
172 division, were ~3-fold lower than WT (Fig. 2d). This effect at an earlier stage of sporulation is consistent
173 with transcriptional analyses indicating that *C. difficile spoVD* and *spoVE* are expressed immediately at
174 the onset of sporulation (Fimlaid et al., 2013; Saujet et al., 2013), in contrast with *B. subtilis spoVD* and
175 *spoVE*, which are expressed in the mother-cell compartment after sporulating cells complete asymmetric
176 division.

177 The decrease in apparent sporulation frequency in Δ*spoVD* and Δ*spoVE* mutants could be due to
178 the enzymes regulating (1) asymmetric division through the synthesis of septal PG and/or (2) sporulation
179 initiation via an unknown mechanism. To rule out the latter possibility, we compared the frequency of
180 sporulation initiation in Δ*spoVD* and Δ*spoVE* cells relative to WT cells. Using a Spo0A-dependent
181 P_{spoIIE}*::mScarlet* transcriptional reporter, we found that Δ*spoVD* and Δ*spoVE* strains activate Spo0A, the
182 master transcriptional regulator that initiates sporulation (Ferrari et al., 1985), at similar frequencies and
183 levels relative to WT (Fig. 2e,f, Supplementary Fig. 6). In contrast, significantly fewer Δ*spoVD* and
184 Δ*spoVE* cells compared to WT induced the expression of a reporter that is activated after the formation of
185 the polar septum (P_{sipL}::*mScarlet*) (Fimlaid et al., 2013; Saujet et al., 2013). Consistent with the reporter
186 data, RT-qPCR and western blot analyses of the Δ*spoVD* and Δ*spoVE* mutants confirmed that they
187 activate Spo0A at WT levels but exhibit defects in activating later-acting sporulation-specific sigma
188 factors that only become activated upon completion of asymmetric division (Supplementary Fig. 7, 8).
189 Overall, our data suggest that *C. difficile* SpoVD and SpoVE play important roles in synthesizing septal
190 PG during asymmetric division, in addition to their canonical function in synthesizing the spore cortex.
191 Consistent with this model, we detected incomplete polar septum formation in Δ*spoVD* and Δ*spoVE,* but
192 not WT, cells in transmission electron microscopy analyses (Fig. 2g). Moreover, in agreement with a
193 previous study (Alabdali et al., 2021)., SpoVD localizes to polar septa during asymmetric division
194 (Supplementary Fig. 9).

195 **Conserved divisome components regulate cell division during spore formation but not vegetative**
196 **growth in *C. difficile*.**

197 Septal PG synthesis requires the coordinated assembly and localization of numerous divisome
198 components at the division site. If SpoVD and SpoVE mediate septal PG synthesis during asymmetric
199 division, we reasoned that their activities are likely regulated by components of the divisome. Previous
200 studies have implicated the widely conserved divisome sub-complex composed of FtsL, FtsQ, and FtsB
201 (also known as FtsL, DivIB, and DivIC in some Firmicutes) in directly regulating the activity and

202 localization of FtsW-FtsI (Levin & Losick, 1994; Daniel et al., 1998; Katis & Wake, 1999; Tsang &
203 Bernhardt, 2015; Marmont & Bernhardt, 2020). Intriguingly, although *C. difficile* appears to lack
204 functional FtsW and FtsI orthologs, it encodes orthologs of their regulators (Supplementary Fig. 10).
205 *cd630_26570* and *cd630_26500* are both located in conserved locations within the *dcw* cluster (Fig. 1a)
206 and encode putative membrane proteins with homology to FtsL and FtsQ, respectively. We also identified
207 *cd630_34920* as encoding an FtsB homolog. We refer to these genes as *ftsL* (*cd630_26570*), *ftsQ*
208 (*cd630_26500*), and *ftsB* (*cd630_34920*) from hereon (Supplementary Fig. 10).
209 Although *ftsL*, *ftsQ*, and *ftsB* encode proteins that are typically considered essential components
210 of the divisome, a previous transposon screen in *C. difficile* identified these genes as non-essential but
211 important for spore formation (Dembek et al., 2015). Consistent with this finding, we readily obtained
212 Δ*ftsL*, Δ*ftsQ,* and Δ*ftsB* deletion strains. These mutants showed no significant growth or morphological
213 defects (Fig. 3a, b), indicating that FtsL, FtsQ, and FtsB likely fulfill non-canonical, sporulation-specific
214 roles in *C. difficile*. Indeed, all three mutants formed heat-resistant spores less efficiently than WT, with
215 Δ*ftsL* and Δ*ftsB* showing ~100-fold defects, respectively, and Δ*ftsQ* showing a modest ~2-fold decrease
216 (Supplementary Fig. 3). These sporulation defects could be complemented by expressing wildtype copies
217 of their respective genes from a chromosomal ectopic locus (Supplementary Fig. 3). The milder
218 phenotypes observed for Δ*ftsQ* are consistent with prior observations that FtsQ is only conditionally
219 essential or completely absent in some bacterial species (Beall & Lutkenhaus, 1989; Le Gouëllec et al.,
220 2008; Masson et al., 2009). Notably, phase-contrast microscopy of sporulating cells revealed that all three
221 mutants form phase-bright spores, albeit infrequently, and TEM analysis confirmed that the mutants can
222 synthesize cortex PG, unlike Δ*spoVD* and Δ*spoVE* cells (Supplementary Fig. 4). However, similar to
223 Δ*spoVD* and Δ*spoVE* strains, incomplete polar septa were detected in TEM analyses of Δ*ftsL,* Δ*ftsQ*, and
224 Δ*ftsB* strains, suggesting that these proteins are important for completing asymmetric division
225 (Supplementary Fig. 4b).
226 Consistent with this observation, cytological profiling revealed that sporulating Δ*ftsL*, *ftsQ*, and
227 Δ*ftsB* cells complete and progress beyond asymmetric division at a significantly lower frequency
228 compared to WT (Fig. 3c, d, Supplementary Fig. 5). A small proportion (~2%) of Δ*ftsL* and Δ*ftsB* cells
229 were able to progress beyond engulfment to make mature spores (Fig. 3d). The phenotype for Δ*ftsQ* was
230 slightly less severe than for Δ*ftsL* and Δ*ftsB*, with ~4% of Δ*ftsQ* cells making phase-bright (cortex-
231 positive) spores (Fig. 3d). However, a higher proportion of Δ*ftsQ* sporulating cells remained stalled at
232 asymmetric division, suggesting that *C. difficile* FtsQ shares similar functions with *B. subtilis* DivIB in
233 regulating PG transformations during engulfment (Thompson et al., 2006) Since the PG synthesizing
234 activity of FtsW-FtsI has been shown to depend on direct interactions between the enzymes and the
235 ternary FtsLQB sub-complex in other bacteria, we tested whether SpoVD and SpoVE form a divisome-

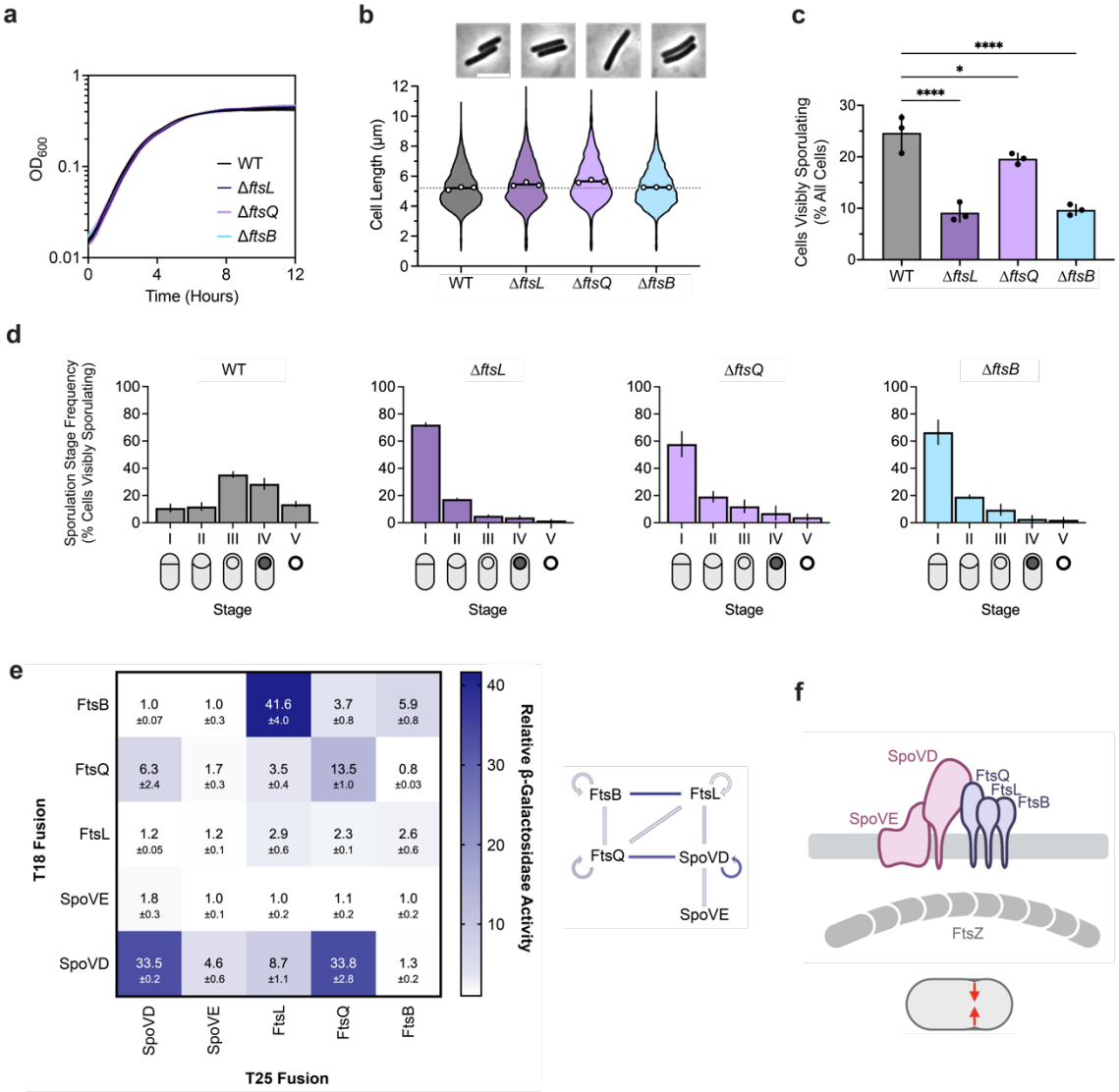

Fig. 3 | The canonical divisome components, FtsL, FtsQ, and FtsB, are dispensable for vegetative cell division but are important for asymmetric division. a, Growth profiles of WT, Δ*ftsL,* Δ*ftsQ*, and Δ*ftsB* strains in BHIS. Data are from a single growth curve experiment; mean, and standard deviation curves are plotted from three biological replicates. **b,** Violin plots showing cell length distributions and representative micrographs of WT, Δ*ftsL,* Δ*ftsQ*, and Δ*ftsB* cells sampled from BHIS cultures during exponential growth (OD_{600} ~0.5). White circles indicate means from each replicate, black lines indicate average means, and the dotted line indicates the WT average mean for comparison across strains. Data from three biological replicates; >1,500 cells per sample. Scale bar, 5 µm. **c, d,** Cytological profiling of sporulating WT, Δ*ftsL,* Δ*ftsQ*, and Δ*ftsB* cells as in Fig. 2 c, d. Bars indicate means, and error bars indicate standard deviation. *p<0.05, ***p<0.0001; statistical significance was determined using an ordinary one-way ANOVA with Dunnett's test. Data from three independent experiments; >1,000 total cells and >100 visibly sporulating cells per sample. **e,** Bacterial two-hybrid analysis of interactions between components of the predicted polar divisome. The β-galactosidase activity was normalized to the negative control. Mean ± standard deviation from three biological replicates is indicated. The schematic shows interactions between different proteins where lines are colored according to the amount of β-galactosidase activity detected. **f,** Schematic showing FtsL, FtsQ, and FtsB forming a divisome-like subcomplex with SpoVD and SpoVE. This polar divisome contributes to septal PG synthesis during asymmetric division.

252 like complex with FtsL, FtsQ, and FtsB by probing pairwise interactions using bacterial two-hybrid
253 assays. This assay confirmed that SpoVD and SpoVE interact, consistent with these enzymes forming a
254 cognate SEDS-bPBP pair as previously shown in *B. subtilis* (Fay et al., 2010) (Fig. 3e,f) and that *C.*
255 *difficile* FtsL, FtsQ, and FtsB likely form a ternary sub-complex similar to homologs in other bacteria (Di
256 Lallo et al., 2003; Karimova et al., 2005; Maggi et al., 2008; Robichon et al., 2008). Importantly, we
257 observed that *C. difficile* SpoVD interacts with FtsL and FtsQ, suggesting that the ternary sub-complex
258 likely directly regulates the activity of SpoVE-SpoVD. Taken together, these data strongly suggest that *C.*
259 *difficile* assembles a distinct polar divisome that partially relies on the sporulation-specific SEDS-bPBP
260 pair, SpoVE-SpoVD, to synthesize the polar septum during endospore formation.

261 **The sole essential SEDS-bPBP pair in *C. difficile* is involved in cell elongation**

262 Although septal PG synthesis by SpoVD and SpoVE is important for asymmetric division, *C. difficile*
263 cells that lack these proteins are still able to synthesize polar septa, albeit at lower rates. It is likely that
264 the PG synthases that mediate vegetative cell division also contribute to septal PG synthesis during
265 asymmetric division. Since *C. difficile* appears to lack obvious orthologs of the widely conserved
266 divisome-specific SEDS-bPBP pair, we considered the involvement of all major PG synthases encoded in
267 the *C. difficile* genome. *C. difficile* has a relatively minimal set of PG synthases: a single class A PBP
268 (PBP1 encoded by *cd630_07810*), three class B PBPs (PBP2, encoded by *cd630_11480*; PBP3, encoded
269 by *cd630_12290*; and SpoVD), two SEDS proteins (RodA, encoded by *mrdB*, and SpoVE), and one
270 monofunctional glycosyltransferase (MGT encoded by *cd630_23930*) (Fig. 4a). Among these synthases,
271 we considered PBP1, PBP2, and RodA to be the most likely candidates for enzymes that contribute to
272 septal PG synthesis during medial division since genes encoding these proteins were previously identified
273 as being essential for vegetative growth (Dembek et al., 2015). Consistent with this and the prior finding
274 that loss of PBP3 results in a sporulation defect (Srikhanta et al., 2019), we confirmed that single
275 deletions of genes encoding PBP3 and MGT do not significantly alter the growth of vegetative cells,
276 although they induce a modest increase in cell length (Supplementary Fig. 11).

277 Although RodA and PBP2 are the sole essential SEDS-bPBP pair, the genomic location of their
278 respective genes adjacent to the *mreBCD* operon, which encodes critical components of the elongasome,
279 predicts that they mediate elongation based on analyses in other bacteria (Meeske et al., 2016).
280 Furthermore, *C. difficile* RodA branches with SEDS enzymes implicated in mediating cell elongation in
281 other organisms and in a separate group from *dcw*-encoded SEDS (Supplementary Fig. 2a, b), consistent
282 with recent work suggesting that the functional divergence of SEDS paralogs to roles in cell division or
283 elongation predates the Last Bacterial Common Ancestor (Megrian et al., 2022). To experimentally

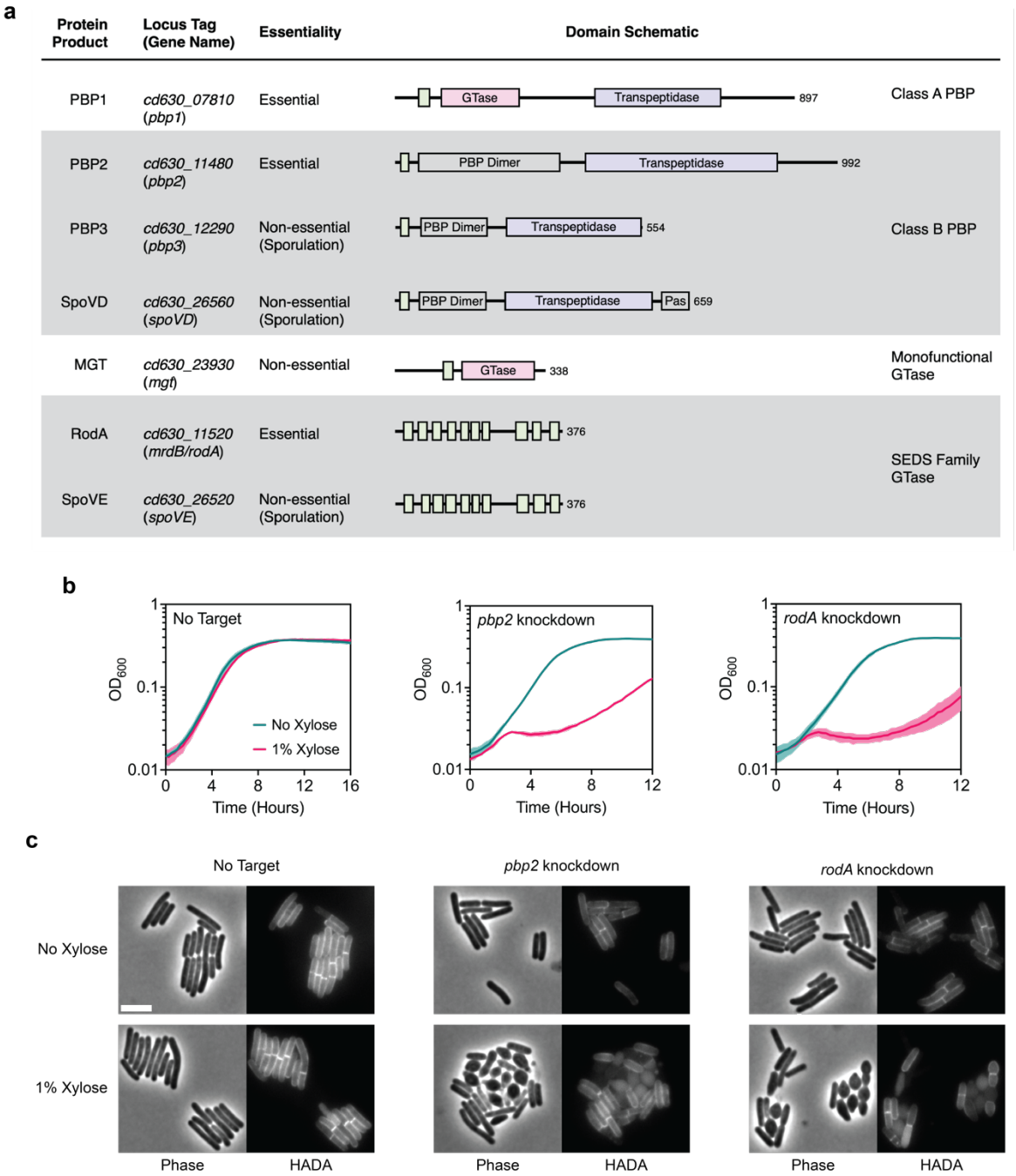

Fig. 4 | RodA and PBP2 are involved in cell elongation. a, Major PG synthases encoded in the *C. difficile* strain 630 genome. Protein domains and catalytic sites predicted using HMMER are indicated in the schematic for each protein (hmmer.org). GTase: Glycosyltransferase Domain (Pink), PBP Dimer: PBP Dimerization Domain, Pas: PASTA Domain, Transpeptidase domain (Purple). Predicted transmembrane regions are depicted as green boxes. b, Growth profiles of *pbp2* and *rodA* CRISPRi knockdown strains compared to a no target control strain. Data are from a single growth curve experiment; mean and standard deviation plotted from three biological replicates. c, Representative micrographs showing morphological and PG incorporation phenotypes of control, *pbp2,* and *rodA* knockdown cells. PG was labeled by incubation with a fluorescent D-amino acid (HADA). Scale bar, 5 µm. Data representative of multiple independent experiments.

293 confirm the roles of RodA and PBP2 in cell elongation, we used CRISPR interference (CRISPRi) (Müh et
294 al., 2019) to knock down the expression of their respective genes. Consistent with their essentiality,
295 individual knockdowns produced significant growth defects upon induction of the CRISPR system (Fig.
296 4b). CRISPRi knockdown of either *rodA* or *pbp2* resulted in lateral bulging, rounding, and frequent lysis
297 of cells (Fig. 4c). These phenotypes are characteristic of cells defective in cell elongation as observed in
298 other rod-shaped bacteria (Henriques et al., 1998; Matsuzawa et al., 1973; Murray et al., 1997; Rismondo
299 et al., 2019; Spratt, 1975) and stand in contrast to the phenotypes of divisome component CRISPRi
300 knock-downs, which induce filamentation due to defects in septum formation. Thus, RodA and PBP2 are
301 the core PG synthases during cell elongation in *C. difficile*.

302 **The *C. difficile* aPBP, PBP1, is the major septal PG synthase during vegetative division**
303 These analyses left the aPBP, PBP1, as the primary candidate for synthesizing septal PG during
304 vegetative division in *C. difficile*. Since aPBPs are capable of both polymerizing and cross-linking PG,
305 PBP1 should be able to substitute for both enzymatic activities fulfilled by a divisome-associated SEDS-
306 bPBP pair. Indeed, PBP1 was previously suggested to be essential for vegetative growth (Dembek et al.,
307 2015), and its depletion results in cell filamentation (Müh et al., 2019). Knockdown of the gene encoding
308 PBP1 validated these prior reports, as it resulted in severe growth defects and cell filamentation
309 phenotypes characteristic of cells deficient in cell division (Fig 5a, b). Moreover, subcellular localization
310 of PBP1 during vegetative growth showed significant enrichment at division septa (Fig. 5e,f).
311 Chemical inhibition of PBP1 activity with the glycosyltransferase inhibitor moenomycin also
312 produced filamentous cells, suggesting a crucial role of PBP1 glycosyltransferase activity in cell division
313 (Fig. 5d). These data contradict a prior report (Cheng et al., 2008), which suggested that *C. difficile* cells
314 are intrinsically resistant to moenomycin. Although moenomycin also inhibits the catalytic activity of
315 monofunctional glycosyltransferases, sensitivity to moenomycin was unchanged in an MGT-null mutant,
316 suggesting that the drastic phenotypes observed in moenomycin-treated cells are exclusively due to the
317 inhibition of PBP1 activity (Supplementary Fig. 12a). Consistent with this, growth defects from
318 moenomycin treatment were rescued by overproduction of PBP1 (Supplementary Fig. 12c). Furthermore,
319 *C. difficile* is sensitive to PBP1 overproduction likely due to dysregulation of PBP1 activity.
320 Next, we considered whether components of the polar divisome described above contribute to
321 vegetative cell division. We reasoned that if this was the case, mutants lacking these components should
322 be hypersensitive to moenomycin treatment. We found that the susceptibility of Δ*spoVD*, Δ*spoVE*, Δ*ftsL*,
323 Δ*divIB*, and Δ*divIC* cells to moenomycin is unchanged compared to WT (Supplementary Fig. 12a,b).
324 Overall, these results are consistent with a non-canonical divisome composition in *C. difficile,* where
325 PBP1 is the major septal PG synthase during vegetative cell division.

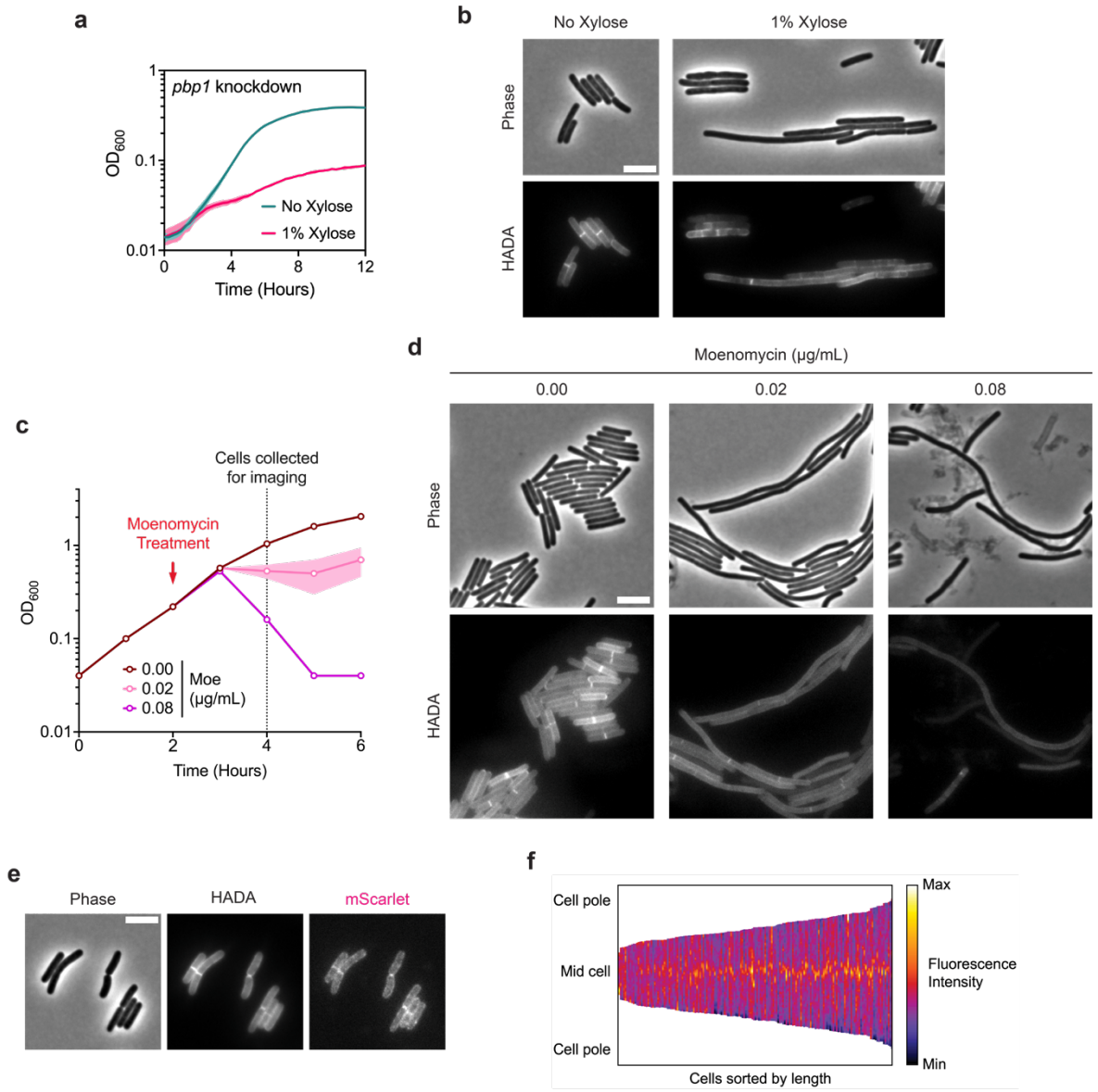

Fig. 5 | The class A PBP, PBP1, is critical for cell division. a, Growth profile of the CRISPRi *pbp1* knockdown strain. Data from a single growth curve experiment; mean and standard deviation plotted from three biological replicates. **b,** Representative micrographs showing morphological and PG incorporation phenotypes of *pbp1* knockdown cells. PG was labeled by incubation with HADA. Scale bar, 5 µm. Data representative of multiple experiments. **c,** Moenomycin treatment of WT cultures. Moenomycin was added after two hours of growth as indicated, and cells were collected and fixed for imaging 2 hours after treatment. Mean and range are plotted from two biological replicates. **d,** Representative micrographs showing morphological and PG incorporation phenotypes of moenomycin-treated WT cells. PG was labeled by incubation with HADA. Scale bar, 5 µm. **e,** Representative phase-contrast and fluorescence micrographs showing PG incorporation and subcellular localization of mScarlet-PBP1 in exponentially growing cells. PG was labeled by incubation with HADA, and *mScarlet-pbp1* was expressed using the native *pbp1* promoter from an ectopic locus. Scale bar, 5 µm. **f,** Demograph showing fluorescence intensity across multiple cells representing subcellular localization of PBP1 in exponentially growing cells. Cells are aligned at the mid-cell and sorted by length. Data are from 173 cells from one experiment and are representative of multiple experiments.

340 **Discussion**

341 The *dcw* cluster is well-conserved across all known bacterial phyla and was likely encoded in the Last
342 Bacterial Common Ancestor (Megrian et al., 2022). While the order and composition of core *dcw* genes
343 involved in PG synthesis and cell division have remained largely unchanged through billions of years of
344 vertical inheritance, our analyses suggest that two key constituents of the cluster, *ftsW* and *ftsI*, have
345 undergone a surprising functional divergence during the evolution of endospore formation. Rather than
346 encoding the core PG synthases required for cell division as they do in most bacteria, the SEDS and bPBP
347 genes in the *dcw* cluster of sporulating Firmicutes likely encode enzymes that become specialized to
348 function exclusively during endospore formation, i.e. as SpoVE and SpoVD. This conclusion is supported
349 by our finding that Firmicutes predicted to have lost the ability to sporulate also lack SEDS genes from
350 their *dcw* cluster (Fig. 1, Supplementary Fig. 1, Supplementary Table 3). Furthermore, we show that, like
351 *B. subtilis* (Daniel et al., 1994; Fay et al., 2010), the SEDS and bPBP genes in the *C. difficile dcw* cluster
352 play sporulation-specific roles (Fig. 2).

353 However, in contrast with *B. subtilis*, where SpoVE and SpoVD function exclusively during
354 cortex synthesis, we have identified a novel role for SpoVE and SpoVD in mediating septal PG synthesis
355 during asymmetric division in *C. difficile*. We posit that this additional function for SpoVE and SpoVD
356 reflects their ancestral role in cell division. Since the last common ancestor of the Firmicutes is thought to
357 have been a spore-former (Garcia et al., 2021), it is likely that this ancestor diversified the function of its
358 *dcw*-encoded cell division PG synthases, FtsW and FtsI, to include both asymmetric division and cortex
359 formation.

360 According to this evolutionary scenario, *C. difficile* SpoVE and SpoVD represent an intermediate
361 form that has retained its involvement in asymmetric division and cortex synthesis, while *B. subtilis*
362 SpoVE and SpoVD became exclusively specialized for cortex synthesis. This interpretation is supported
363 by our data suggesting that the PG synthesizing function of *C. difficile* SpoVD and SpoVE during
364 asymmetric division is regulated by the divisome components FtsL, FtsQ, and FtsB (Fig. 3), which are
365 essential regulators of FtsW and FtsI in other organisms, including *B. subtilis* (Levin & Losick, 1994;
366 Daniel et al., 1998; Katis & Wake, 1999; Tsang & Bernhardt, 2015; Marmont & Bernhardt, 2020).

367 Notably, the specialization of *dcw*-encoded SEDS and bPBP enzymes in mediating PG
368 transformations during spore formation in the Firmicutes required that these organisms develop or
369 repurpose other enzymes to drive vegetative cell division. Sporulating members of the Bacilli encode an
370 additional bPBP in the *dcw* cluster adjacent to *spoVD* (Fig. 1), which appears to encode a functional
371 ortholog of FtsI and was likely a product of a gene duplication event. Similarly, the evolution of a
372 functional ortholog of FtsW encoded outside the *dcw* cluster in the Bacilli was likely facilitated by a gene

373 duplication or horizontal gene transfer event. In contrast, many members of the Clostridia appear to lack
374 *ftsW* and *ftsI* orthologs (Fig. 1), so a non-SEDS-bPBP PG synthase, namely the aPBP, PBP1, likely
375 evolved to mediate cell division independent of the canonical cell division machinery.
376 While it is unclear why the function of SpoVE and SpoVD during asymmetric division is not
377 conserved in *B. subtilis* and likely other Bacilli, it appears that their roles in this critical process will likely
378 be observed only in spore formers that lack functional FtsW and FtsI orthologs. This is consistent with
379 our observation that, unlike *C. difficile* and most other Clostridia, the Bacilli and Negativicutes appear to
380 encode functional orthologs of FtsW and FtsI (Fig 1), which likely mediate both medial and asymmetric
381 division. Interestingly, the *B. subtilis* aPBP PBP1 is required for efficient septation during asymmetric
382 division but not medial division (Scheffers & Errington, 2004), similar to SpoVE-SpoVD requirement for
383 efficient asymmetric division in *C. difficile*. These observations suggest that the formation of the division
384 septum during asymmetric division may have additional requirements for both aPBP and SEDS-bPBP
385 activities, which may contribute to the differences between medial and asymmetric septa observed in *B.*
386 *subtilis* (Khanna et al., 2021).
387 While our results strongly suggest that the essential PG synthases in *C. difficile*, PBP1 and RodA-
388 PBP2, are functionally specialized to mediate cell division and elongation, respectively (Fig. 4, 5), it
389 remains possible that these two distinct sets of PBPs participate in both processes. Indeed, PBP1 likely
390 contributes to general cell wall synthesis and maintenance independent of its role in septation, given that
391 aPBPs in other bacteria can function autonomously from the divisome (Vigouroux et al., 2020). This is
392 supported by our observation of lower levels of HADA incorporation throughout the cell upon *pbp1*
393 knockdown or moenomycin treatment (Fig. 5b, d). Furthermore, a recent study suggests that *C. difficile*
394 PBP1 transpeptidase activity is likely non-essential (Sacco et al., 2022), in which case, PBP2 may provide
395 the missing transpeptidase activity. Indeed, redundancy in transpeptidase activities during cell division
396 has been described in *B. subtilis* and *S. aureus* and may be more widely conserved than currently
397 appreciated (Pinho et al., 2001; Reichmann et al., 2019; Sassine et al., 2017; Wacnik et al., 2022).
398 Crucially, whether and how *C. difficile* PBP1 activity is regulated during septal PG synthesis remains
399 unclear. FtsL, FtsQ, and FtsB are dispensable during vegetative growth (Fig 3), and *C. difficile* lacks
400 homologs of FtsA and FtsN, which regulate divisome assembly and PG synthesis activity in many
401 bacteria (Egan et al., 2020). Thus, factors that substitute for the function of these widely conserved
402 divisome proteins remain to be discovered. Interestingly, a cluster of three genes encoding mid cell-
403 localizing proteins (MldABC) unique to *C. difficile* and closely related organisms appear to be important
404 for cell division (Ransom et al., 2014). Since one of these proteins (MldA) contains a PG-binding SPOR
405 domain which is commonly found in components of the divisome in other bacteria and was recently
406 implicated in regulating aPBP activity in *E. coli* (Pazos et al., 2020), Mld proteins may be involved in

407 regulating septal PG synthesis by PBP1. However, further study is required to define the components of
408 the distinct divisome encoded by *C. difficile*.
409 Altogether, our findings provide novel insight into the evolution of PG-synthesizing enzymes in
410 the Firmicutes and highlight the diversity of PG synthesis mechanisms employed by bacteria. The
411 observations may explain some of the disparities in cell division mechanisms reported for model
412 Firmicutes organisms such as *B. subtilis* and *S. aureus* compared to non-Firmicutes models such as *E.*
413 *coli,* including differences in FtsW-FtsI enzyme dynamics and aPBP function in relation to the divisome
414 (Egan et al., 2020; Straume et al., 2021). Moreover, by revealing unique characteristics of *C. difficile*'s
415 cell division machinery during sporulation and vegetative growth, these analyses may inform the
416 development of more specific therapeutics against this important pathogen.

Methods

Gene synteny, homology searches, and phylogenetic analyses

Genomic loci containing *dcw* clusters shown in Fig. 1 were manually determined by searching for *dcw* genes (*mraZ*, *ftsW*/*spoVE*, *ftsZ*) and extracted from genomes (accession numbers and coordinates are listed in Supplementary Table S1). Gene neighborhoods were visualized using Clinker (Gilchrist & Chooi, 2021) on the CAGECAT web server (https://cagecat.bioinformatics.nl/tools/clinker) (van den Belt et al., 2023).

For all other analyses presented in Supplementary Fig. 1 & 2 and Supplementary Table 3, we assembled a local databank of Firmicutes by selecting one proteome per genus as previously described (Luhur et al., 2020). Proteome selection was realized considering genome characteristics such as assembly level and category. The assembled databank contains 494 genomes listed in Supplementary Table 2. In order to build a reference phylogeny, exhaustive HMM-based homology searches (with the option --cut_ga) were carried out by using HMM profiles of bacterial ribosomal proteins from the Pfam 29.0 database as queries on the Firmicutes databank using the HMMER-3.1b2 package (hmmer.org) (Johnson et al., 2010). The conserved ribosomal proteins were aligned with MAFFT-v7.407 with the auto option and trimmed using BMGE-1.1 (Criscuolo & Gribaldo, 2010). The resulting trimmed alignments were concatenated into a supermatrix (497 taxa and 3,776 amino acid positions). A maximum likelihood tree was generated using IQTREE-1.6.3 (Nguyen et al., 2015) under the LG+I+G4 model with 1000 ultrafast bootstrap replicates.

Homology searches were performed using HMMSEARCH from the HMMER-3.1b2 package to screen all the proteomes in the Firmicutes databank for the presence of Spo0A, SpoIIE, SEDS glycosyltransferases, and bPBP homologs. We used the Pfam database to retrieve Pfam domains PF08769, PF07228, PF01098, and PF00905 for Spo0A, SpoIIE, SEDS glycosyltransferases, and bPBP respectively (Finn et al., 2016). All hits were then manually curated using phylogeny and domain organization to discard false positives. For SEDS and bPBP sets of hits, the kept sequences were aligned with MAFFT v7.481 (--auto) (Katoh & Standley, 2013), trimmed with trimAl 1.2rev59 (Capella-Gutiérrez et al., 2009) and single gene trees were build using IQ-TREE v2.0.7 (Minh et al., 2020) with best-fit model chosen according to BIC criterium.

We next used MacSyFinder2 (Néron et al., 2023) to locate the hits in the genomes. We assessed the genes as located in the dcw cluster when at least four out of the genes *ftsW*/*spoVE*, *ftsI*/*spoVD*, *ftsA*, *mraW*, *mraY*, *ftsZ*, *mraZ,* and *murCDEF* cooccurred in the genome separated by no more than five other genes. The *rodA*-*mrdA* pair located out of the dcw cluster was assessed when they were found separated by no more than five other genes with the absence of *mraW* and *mraY* in their close synteny. Finally, we

450 identified the pair *ftsW-pycA* when the two genes cooccurred in the genome, separated by no more than 3
451 other genes. The presence or absence of the studied proteins and their synteny in the genomes were
452 mapped onto the trees using IToL(Letunic & Bork, 2021).
453 The Jaccard similarity coefficients reported in Supplementary Table 3 were calculated using R
454 and RStudio software using the dataset from Supplementary Table 2. The Jaccard similarity coefficient
455 for each pairwise comparison was calculated by dividing the number of shared organisms by the total
456 number of organisms in the two sets being compared.

457 ***C. difficile* strain construction and growth conditions**
458 All *C. difficile* strains used in the study are derivatives of 630Δ*erm*. Mutant strains were constructed in a
459 630Δ*erm*Δ*pyrE* strain using *pyrE*-based allele-coupled exchange as previously described (Ng et al.,
460 2013). All strains used in the study are reported in Supplementary Table 4. *C. difficile* strains were grown
461 from frozen glycerol stocks on brain heart infusion-supplemented (BHIS) agar plates with taurocholate
462 (TA, 0.1% w/v). *C. difficile* strains harboring pIA33- or pRPF185-based plasmids were grown on media
463 supplemented with thiamphenicol (10 µg/mL in liquid cultures and 5 µg/mL in agar plates). Cultures
464 were grown at 37°C under anaerobic conditions using a gas mixture containing 85% N2, 5% CO2, and
465 10% H2.

466 ***E. coli* strain constructions**
467 Supplementary Table 5 lists all plasmids used in the study, with links to plasmid maps containing all
468 primer sequences used for cloning. Plasmids were cloned via Gibson assembly, and cloned plasmids were
469 transformed into *E. coli* (DH5α or XL1-Blue strains). All plasmids were confirmed by sequencing the
470 inserted region. Confirmed plasmids were transformed into the *E. coli* HB101 strain for conjugation with
471 *C. difficile*. All *E. coli* HB101 strains used for conjugation are also listed in Supplementary Table 5.

472 **Plate-based sporulation assays**
473 For assays requiring sporulating cells, cultures were grown to early stationary phase, back-diluted 1:50
474 into BHIS, and grown until they reached an OD_{600} between 0.35 and 0.75. 120 µL of this culture was
475 spread onto 70:30 (70% SMC media and 30% BHIS media) or SMC agar plates as indicated (40 ml media
476 per plate). Sporulating cells were scraped from the plate and collected into phosphate-buffered saline
477 (PBS), and sporulation levels were visualized by phase-contrast microscopy as previously described
478 (Pishdadian et al., 2015).

479 **Heat resistance assay**

480 Heat-resistant spore formation was measured 18-22 hours after sporulation induction on 70:30 agar plates,
481 as previously described (Fimlaid et al., 2015). Heat-resistance efficiencies represent the average ratio of
482 heat-resistant colony-forming units (CFUs) to total CFUs for a given strain relative to the average ratio
483 for the wild-type strain.

484 **Western blot analysis**

485 Samples were collected 17 hours after sporulation induction on 70:30 agar plates and processed for
486 immunoblotting as previously described. σ^F, $\sigma^{E,}$ and Spo0A were resolved using 15% SDS–
487 polyacrylamide gel electrophoresis (SDS–PAGE) gels, whereas SpoVD and SpoIVA were resolved using
488 12% SDS–PAGE gels. Proteins were transferred to polyvinylidene difluoride membranes, which were
489 subsequently probed with rabbit (anti-σ^F, anti-σ^E, and anti-SpoVD) and mouse (anti-Spo0A and anti-
490 SpoIVA) polyclonal primary antibodies, and anti-rabbit IR800 and anti-mouse IR680 secondary
491 antibodies (LI-COR). Blots were imaged using a LiCor Odyssey CLx imaging system. The results shown
492 are representative of multiple experiments.

493 **RT-qPCR analysis**

494 RNA was harvested from sporulating cells 10-11 hours after sporulating induction on 70:30 agar plates.
495 Total RNA was processed as previously described (Fimlaid et al., 2013) using a MICROBExpress
496 Bacterial mRNA Enrichment Kit for mRNA enrichment. Transcript levels were determined from cDNA
497 templates prepared from a single experiment with three biological replicates per sample. Gene-specific
498 primer pairs are provided in Supplementary Table 6. RT–qPCR was performed as previously described
499 (Oliveira et al., 2020), using iTaq Universal SYBR Green supermix (BioRad), 50 nM of gene-specific
500 primers, and an Mx3005P qPCR system (Stratagene) in a total volume of 25 µL. The following cycling
501 conditions were used: 95 °C for 2 min, followed by 40 cycles of 95 °C for 15 s and 60 °C for 1 min.
502 Statistical tests were performed using GraphPad Prism (GraphPad Software, San Diego, CA, USA).

503 **Bacterial two-hybrid analyses**

504 Bacterial adenylate cyclase two-hybrid (BACTH) assays were performed using E. coli BTH101 cells
505 based on the system first described by Karimova et al. (Karimova et al., 2005). Briefly, BTH101 cells
506 were freshly transformed with 100 ng of each BACTH assay plasmid and plated on fresh LB agar plates
507 supplemented with 50 µg/ml kanamycin, 100 µg/ml Ampicillin, and 0.5 mM isopropyl β-D-
508 thiogalactopyranoside (IPTG). Plates were incubated for 64-68 hours at 30°C, and β-galactosidase
509 activity was quantified in Miller units as previously described. The β-galactosidase activity of cells

510 transformed with the empty pUT18C and pKT25 vectors was used as a negative control for
511 normalization.

512 **Growth curve assays**

513 For each replicate of the growth assay shown in Figure 5c, a mid-log culture was normalized to a starting
514 OD_{600} ~0.05. After two hours of growth, the culture was aliquoted into three separate tubes and
515 supplemented with moenomycin as indicated. The OD_{600} value of each culture was measured every hour
516 using a portable colorimeter (Biochrom WPA CO7500). For all other growth assays, stationary phase
517 cultures were back-diluted 1:50 in BHIS and grown to mid-log phase (OD_{600} 0.5). Log-phase cultures
518 were normalized to a starting OD_{600} ~0.01 and distributed into wells (150µL per well) of a 96-well plate.
519 The plate was incubated in an Epoch microplate spectrophotometer (Agilent BioTek) at 37˚C with linear
520 shaking for 2 mins prior to each time point. The OD_{600} value for each well was recorded every 15 minutes.
521 For growth assays involving strains with pIA33- or pRPF185-based plasmids, media was supplemented
522 with 10 µg/mL thiamphenicol and either 1% xylose or anhydrotetracycline as indicated. For assays
523 involving moenomycin treatment, cultures were supplemented with different concentrations of
524 moenomycin as indicated.

525 **Nucleoid, membrane, and cell wall labeling**

526 Fluorescence microscopy was performed on sporulating cells using Hoechst 33342 (Molecular Probes;
527 15 $\mu g\ ml^{-1}$) and FM4-64 (Invitrogen; 1 $\mu g\ ml^{-1}$) to stain nucleoid and membrane, respectively. For cell
528 wall labeling, HADA (Tocris Bioscience) was added to exponentially growing cell culture to a final
529 concentration of 50-100 µM and incubated for ~2 mins before cell fixation.

530 **Cell fixation**

531 Cells were fixed as previously described (Ransom et al., 2016). In brief, 800 µL of cell suspension was
532 added to 200 µL of a 5× fixation solution containing paraformaldehyde and $NaPO_4$ buffer. Samples were
533 mixed and incubated in the dark for 30 min at room temperature, followed by 30 min on ice. Fixed cells
534 were washed three times in phosphate-buffered saline (PBS) and resuspended in an appropriate volume of
535 PBS depending on cellular density. Cells were imaged within 72 hours after fixation.

536 **Microscope Hardware**

537 All samples for a given experiment were imaged from a single agar pad (1.5% low-melting point agarose
538 in PBS). Phase-contrast micrographs shown in Supplementary Fig. 3 were acquired using a Zeiss
539 Axioskop upright microscope with a 100× Plan-NEOFLUAR oil-immersion phase-contrast objective and

540 a Hamamatsu C4742-95 Orca 100 CCD Camera. All other phase-contrast and fluorescence micrographs
541 were obtained using a Leica DMi8 inverted microscope equipped with a 63× 1.4 NA Plan Apochromat
542 oil-immersion phase-contrast objective, a high precision motorized stage (Pecon), and an incubator
543 (Pecon) set at 37˚C. Excitation light was generated by a Lumencor Spectra-X multi-LED light source with
544 integrated excitation filters. An XLED-QP quadruple-band dichroic beam-splitter (Leica) was used
545 (transmission: 415, 470, 570, and 660 nm) with an external filter wheel for all fluorescent channels. FM4-
546 464 was excited at 550/38 nm with, and emitted light was filtered using a 705/72-nm emission filter
547 (Leica); HADA and Hoechst were excited at 395/40, and emitted light was filtered using a 440/40-nm
548 emission filter (Leica); mScarlet was excited at 550/38 nm with, and emitted light was filtered using a
549 590/50-nm emission filter (Leica). Emitted and transmitted light was detected using a Leica DFC 9000
550 GTC sCMOS camera. 1- to 2-µm z-stacks were taken when needed with 0.21-µm z-slices.

551 **Microscopy image analyses**

552 Images were acquired and exported using the LASX software. To avoid bleed-through of fluorescent
553 signal into neighboring cells, a background subtraction method (Leica Instant Computational Clearing)
554 was applied to the fluorescence images used for fluorescent reporter analyses shown in Fig. 2 f,g and
555 Supplementary Fig. 5. All other images were exported without further processing. After export, images
556 were processed using Fiji (Schindelin et al., 2012) to remove out-of-focus regions via cropping. The best-
557 focused Z-planes for all channels were manually selected to correct for any chromatic aberration. Image
558 scaling was adjusted to improve brightness and contrast for display and was applied equally to all images
559 shown in a single panel. For cell segmentation and quantification of length and fluorescent intensities, the
560 MATLAB-based image analysis pipeline SuperSegger (Stylianidou et al., 2016) was used with the default
561 60× settings. Visualization of quantified data and any associated statistical tests were performed using
562 GraphPad Prism (GraphPad Software, San Diego, CA, USA).

563 Segmentation of cells and fluorescent intensity analyses used to generate data shown in Fig. 5f to
564 analyze mScarlet-PBP1 localization was conducted using the MicrobeJ plugin (Ducret et al., 2016) in
565 ImageJ. Analyses of SpoVD-mScarlet localization and HADA incorporation in asymmetrically dividing
566 cells shown in Supplementary Fig. 5 were conducted in ImageJ. Individual cells undergoing asymmetric
567 division were isolated by manually identifying cells with a polar septum in the HADA channel. A 5-pixel
568 wide pole-to-pole vector was drawn to gather fluorescent intensities across the cell. For each channel, the
569 fluorescent intensity was normalized to the minimum and maximum values for each cell and plotted
570 against the normalized cell length.

571 **Transmission electron microscopy**

572 Sporulating cells were collected ~22 hours after sporulation induction on 70:30 or SMC agar plates. Cells
573 were fixed and processed for electron microscopy by the University of Vermont Microscopy Center as
574 previously described (Putnam et al., 2013). All TEM images were captured on a JEOL 1400 Transmission
575 Electron Microscope (Jeol USA, Inc., Peabody, MA) with an AMT XR611 high-resolution 11-megapixel
576 mid-mount CCD camera.

577 **Acknowledgments**

578 We acknowledge the University of Vermont Microscopy Imaging Core for processing the samples and
579 acquiring the images for all Transmission Electron Microscopy analyses. We thank Craig D. Ellermeier
580 and David S. Weiss for their input on the project and for sharing protocols and plasmids used in the study.
581 We are grateful to members of the Shen lab for helpful discussions and feedback on the manuscript. The
582 schematic shown in Figure 3f was created using BioRender.com. The National Institute of Allergy and
583 Infectious Diseases grant R01 AI122232 (to A.S.), and Burroughs Wellcome Fund for Investigators in
584 Pathogenesis Award (to A.S.) provided funding for this work.

585 **References**

586 Alabdali, Y. A. J., Oatley, P., Kirk, J. A., & Fagan, R. P. (2021). A cortex-specific penicillin-binding
587 protein contributes to heat resistance in *Clostridioides difficile* spores. *Anaerobe*, *70*, 102379.
588 https://doi.org/10.1016/j.anaerobe.2021.102379
589 Atwal, S., Chuenklin, S., Bonder, E. M., Flores, J., Gillespie, J. J., Driscoll, T. P., & Salje, J. (2021).
590 Discovery of a Diverse Set of Bacteria That Build Their Cell Walls without the Canonical
591 Peptidoglycan Polymerase aPBP. *MBio*, *12*(4), e01342-21. https://doi.org/10.1128/mBio.01342-
592 21
593 Beall, B., & Lutkenhaus, J. (1989). Nucleotide sequence and insertional inactivation of a *Bacillus subtilis*
594 gene that affects cell division, sporulation, and temperature sensitivity. *Journal of Bacteriology*,
595 *171*(12), 6821–6834. https://doi.org/10.1128/jb.171.12.6821-6834.1989
596 Capella-Gutiérrez, S., Silla-Martínez, J. M., & Gabaldón, T. (2009). trimAl: A tool for automated
597 alignment trimming in large-scale phylogenetic analyses. *Bioinformatics*, *25*(15), 1972–1973.
598 https://doi.org/10.1093/bioinformatics/btp348
599 Cheng, T.-J. R., Sung, M.-T., Liao, H.-Y., Chang, Y.-F., Chen, C.-W., Huang, C.-Y., Chou, L.-Y., Wu,
600 Y.-D., Chen, Y.-H., Cheng, Y.-S. E., Wong, C.-H., Ma, C., & Cheng, W.-C. (2008). Domain
601 requirement of moenomycin binding to bifunctional transglycosylases and development of high-
602 throughput discovery of antibiotics. *Proceedings of the National Academy of Sciences*, *105*(2),
603 431–436. https://doi.org/10.1073/pnas.0710868105
604 Cho, H., Wivagg, C. N., Kapoor, M., Barry, Z., Rohs, P. D. A., Suh, H., Marto, J. A., Garner, E. C., &
605 Bernhardt, T. G. (2016). Bacterial cell wall biogenesis is mediated by SEDS and PBP polymerase
606 families functioning semi-autonomously. *Nature Microbiology*, *1*(10), Article 10.
607 https://doi.org/10.1038/nmicrobiol.2016.172
608 Criscuolo, A., & Gribaldo, S. (2010). BMGE (Block Mapping and Gathering with Entropy): A new
609 software for selection of phylogenetic informative regions from multiple sequence alignments.
610 *BMC Evolutionary Biology*, *10*(1), 210. https://doi.org/10.1186/1471-2148-10-210
611 Daniel, R. A., Drake, S., Buchanan, C. E., Scholle, R., & Errington, J. (1994). The *Bacillus subtilis*
612 spoVD gene encodes a mother-cell-specific penicillin-binding protein required for spore
613 morphogenesis. *Journal of Molecular Biology*, *235*(1), 209–220. https://doi.org/10.1016/S0022-
614 2836(05)80027-0
615 Daniel, R. A., Harry, E. J., Katis, V. L., Wake, R. G., & Errington, J. (1998). Characterization of the
616 essential cell division gene ftsL(yIID) of *Bacillus subtilis* and its role in the assembly of the
617 division apparatus. *Molecular Microbiology*, *29*(2), 593–604. https://doi.org/10.1046/j.1365-
618 2958.1998.00954.x
619 Dembek, M., Barquist, L., Boinett, C. J., Cain, A. K., Mayho, M., Lawley, T. D., Fairweather, N. F., &
620 Fagan, R. P. (2015). High-Throughput Analysis of Gene Essentiality and Sporulation in
621 *Clostridium difficile*. *MBio*, *6*(2). https://doi.org/10.1128/mBio.02383-14
622 Di Lallo, G., Fagioli, M., Barionovi, D., Ghelardini, P., & Paolozzi, L. Y. (2003). Use of a two-hybrid
623 assay to study the assembly of a complex multicomponent protein machinery: Bacterial
624 septosome differentiation. *Microbiology*, *149*(12), 3353–3359.
625 https://doi.org/10.1099/mic.0.26580-0
626 Dion, M. F., Kapoor, M., Sun, Y., Wilson, S., Ryan, J., Vigouroux, A., van Teeffelen, S., Oldenbourg, R.,
627 & Garner, E. C. (2019). *Bacillus subtilis* cell diameter is determined by the opposing actions of
628 two distinct cell wall synthetic systems. *Nature Microbiology*, *4*(8), Article 8.
629 https://doi.org/10.1038/s41564-019-0439-0
630 Ducret, A., Quardokus, E. M., & Brun, Y. V. (2016). MicrobeJ, a tool for high throughput bacterial cell
631 detection and quantitative analysis. *Nature Microbiology*, *1*(7), Article 7.
632 https://doi.org/10.1038/nmicrobiol.2016.77

633 Egan, A. J. F., Errington, J., & Vollmer, W. (2020). Regulation of peptidoglycan synthesis and
634 remodelling. *Nature Reviews. Microbiology*, *18*(8), 446–460. https://doi.org/10.1038/s41579-020-
635 0366-3
636 Emami, K., Guyet, A., Kawai, Y., Devi, J., Wu, L. J., Allenby, N., Daniel, R. A., & Errington, J. (2017).
637 RodA as the missing glycosyltransferase in *Bacillus subtilis* and antibiotic discovery for the
638 peptidoglycan polymerase pathway. *Nature Microbiology*, *2*(3), Article 3.
639 https://doi.org/10.1038/nmicrobiol.2016.253
640 Fay, A., Meyer, P., & Dworkin, J. (2010). Interactions Between Late-Acting Proteins Required for
641 Peptidoglycan Synthesis during Sporulation. *Journal of Molecular Biology*, *399*(4), 547–561.
642 https://doi.org/10.1016/j.jmb.2010.04.036
643 Ferrari, F. A., Trach, K., LeCoq, D., Spence, J., Ferrari, E., & Hoch, J. A. (1985). Characterization of the
644 *spo0A* locus and its deduced product. *Proceedings of the National Academy of Sciences of the*
645 *United States of America*, *82*(9), 2647–2651.
646 Fimlaid, K. A., Bond, J. P., Schutz, K. C., Putnam, E. E., Leung, J. M., Lawley, T. D., & Shen, A. (2013).
647 Global analysis of the sporulation pathway of *Clostridium difficile*. *PLoS Genetics*, *9*(8),
648 e1003660. https://doi.org/10.1371/journal.pgen.1003660
649 Fimlaid, K. A., Jensen, O., Donnelly, M. L., Francis, M. B., Sorg, J. A., & Shen, A. (2015). Identification
650 of a Novel Lipoprotein Regulator of *Clostridium difficile* Spore Germination. *PLOS Pathogens*,
651 *11*(10), e1005239. https://doi.org/10.1371/journal.ppat.1005239
652 Finn, R. D., Coggill, P., Eberhardt, R. Y., Eddy, S. R., Mistry, J., Mitchell, A. L., Potter, S. C., Punta, M.,
653 Qureshi, M., Sangrador-Vegas, A., Salazar, G. A., Tate, J., & Bateman, A. (2016). The Pfam
654 protein families database: Towards a more sustainable future. *Nucleic Acids Research*, *44*(D1),
655 D279-285. https://doi.org/10.1093/nar/gkv1344
656 Galperin, M. Y., Yutin, N., Wolf, Y. I., Vera Alvarez, R., & Koonin, E. V. (2022). Conservation and
657 Evolution of the Sporulation Gene Set in Diverse Members of the Firmicutes. *Journal of*
658 *Bacteriology*, *204*(6), e00079-22. https://doi.org/10.1128/jb.00079-22
659 Garcia, P. S., Duchemin, W., Flandrois, J.-P., Gribaldo, S., Grangeasse, C., & Brochier-Armanet, C.
660 (2021). A Comprehensive Evolutionary Scenario of Cell Division and Associated Processes in
661 the Firmicutes. *Molecular Biology and Evolution*, *38*(6), 2396–2412.
662 https://doi.org/10.1093/molbev/msab034
663 Gilchrist, C. L. M., & Chooi, Y.-H. (2021). clinker & clustermap.js: Automatic generation of gene cluster
664 comparison figures. *Bioinformatics*, *37*(16), 2473–2475.
665 https://doi.org/10.1093/bioinformatics/btab007
666 Henriques, A. O., de Lencastre, H., & Piggot, P. J. (1992). A Bacillus subtilis morphogene cluster that
667 includes spoVE is homologous to the mra region of *Escherichia coli*. *Biochimie*, *74*(7–8), 735–
668 748. https://doi.org/10.1016/0300-9084(92)90146-6
669 Henriques, A. O., Glaser, P., Piggot, P. J., & Moran Jr, C. P. (1998). Control of cell shape and elongation
670 by the rodA gene in *Bacillus subtilis*. *Molecular Microbiology*, *28*(2), 235–247.
671 https://doi.org/10.1046/j.1365-2958.1998.00766.x
672 Ikeda, M., Sato, T., Wachi, M., Jung, H. K., Ishino, F., Kobayashi, Y., & Matsuhashi, M. (1989).
673 Structural similarity among Escherichia coli FtsW and RodA proteins and *Bacillus subtilis*
674 SpoVE protein, which function in cell division, cell elongation, and spore formation, respectively.
675 *Journal of Bacteriology*, *171*(11), 6375–6378. https://doi.org/10.1128/jb.171.11.6375-6378.1989
676 Johnson, L. S., Eddy, S. R., & Portugaly, E. (2010). Hidden Markov model speed heuristic and iterative
677 HMM search procedure. *BMC Bioinformatics*, *11*(1), 431. https://doi.org/10.1186/1471-2105-11-
678 431
679 Joyce, G., Williams, K. J., Robb, M., Noens, E., Tizzano, B., Shahrezaei, V., & Robertson, B. D. (2012).
680 Cell Division Site Placement and Asymmetric Growth in Mycobacteria. *PLOS ONE*, *7*(9),
681 e44582. https://doi.org/10.1371/journal.pone.0044582

Karimova, G., Dautin, N., & Ladant, D. (2005). Interaction Network among Escherichia coli Membrane Proteins Involved in Cell Division as Revealed by Bacterial Two-Hybrid Analysis. *Journal of Bacteriology*, *187*(7), 2233–2243. https://doi.org/10.1128/JB.187.7.2233-2243.2005

Katis, V. L., & Wake, R. G. (1999). Membrane-bound division proteins DivIB and DivIC of *Bacillus subtilis* function solely through their external domains in both vegetative and sporulation division. *Journal of Bacteriology*, *181*(9), 2710–2718. https://doi.org/10.1128/JB.181.9.2710-2718.1999

Katoh, K., & Standley, D. M. (2013). MAFFT multiple sequence alignment software version 7: Improvements in performance and usability. *Molecular Biology and Evolution*, *30*(4), 772–780. https://doi.org/10.1093/molbev/mst010

Khanna, K., Lopez-Garrido, J., Sugie, J., Pogliano, K., & Villa, E. (2021). Asymmetric localization of the cell division machinery during *Bacillus subtilis* sporulation. *ELife*, *10*, e62204. https://doi.org/10.7554/eLife.62204

Kieser, K. J., Boutte, C. C., Kester, J. C., Baer, C. E., Barczak, A. K., Meniche, X., Chao, M. C., Rego, E. H., Sassetti, C. M., Fortune, S. M., & Rubin, E. J. (2015). Phosphorylation of the Peptidoglycan Synthase PonA1 Governs the Rate of Polar Elongation in Mycobacteria. *PLoS Pathogens*, *11*(6), e1005010. https://doi.org/10.1371/journal.ppat.1005010

Le Gouëllec, A., Roux, L., Fadda, D., Massidda, O., Vernet, T., & Zapun, A. (2008). Roles of Pneumococcal DivIB in Cell Division. *Journal of Bacteriology*, *190*(13), 4501–4511. https://doi.org/10.1128/JB.00376-08

Leclercq, S., Derouaux, A., Olatunji, S., Fraipont, C., Egan, A. J. F., Vollmer, W., Breukink, E., & Terrak, M. (2017). Interplay between Penicillin-binding proteins and SEDS proteins promotes bacterial cell wall synthesis. *Scientific Reports*, *7*(1), Article 1. https://doi.org/10.1038/srep43306

Letunic, I., & Bork, P. (2021). Interactive Tree Of Life (iTOL) v5: An online tool for phylogenetic tree display and annotation. *Nucleic Acids Research*, *49*(W1), W293–W296. https://doi.org/10.1093/nar/gkab301

Levin, P. A., & Losick, R. (1994). Characterization of a cell division gene from *Bacillus subtilis* that is required for vegetative and sporulation septum formation. *Journal of Bacteriology*, *176*(5), 1451–1459. https://doi.org/10.1128/jb.176.5.1451-1459.1994

Luhur, J., Chan, H., Kachappilly, B., Mohamed, A., Morlot, C., Awad, M., Lyras, D., Taib, N., Gribaldo, S., Rudner, D. Z., & Rodrigues, C. D. A. (2020). A dynamic, ring-forming MucB / RseB-like protein influences spore shape in *Bacillus subtilis*. *PLOS Genetics*, *16*(12), e1009246. https://doi.org/10.1371/journal.pgen.1009246

Maggi, S., Massidda, O., Luzi, G., Fadda, D., Paolozzi, L., & Ghelardini, P. (2008). Division protein interaction web: Identification of a phylogenetically conserved common interactome between Streptococcus pneumoniae and Escherichia coli. *Microbiology*, *154*(10), 3042–3052. https://doi.org/10.1099/mic.0.2008/018697-0

Margolis, P., Driks, A., & Losick, R. (1991). Establishment of Cell Type by Compartmentalized Activation of a Transcription Factor. *Science*, *254*(5031), 562–565. https://doi.org/10.1126/science.1948031

Marmont, L. S., & Bernhardt, T. G. (2020). A conserved subcomplex within the bacterial cytokinetic ring activates cell wall synthesis by the FtsW-FtsI synthase. *Proceedings of the National Academy of Sciences*, *117*(38), 23879–23885. https://doi.org/10.1073/pnas.2004598117

Masson, S., Kern, T., Le Gouëllec, A., Giustini, C., Simorre, J.-P., Callow, P., Vernet, T., Gabel, F., & Zapun, A. (2009). Central Domain of DivIB Caps the C-terminal Regions of the FtsL/DivIC Coiled-coil Rod. *Journal of Biological Chemistry*, *284*(40), 27687–27700. https://doi.org/10.1074/jbc.M109.019471

Matsuzawa, H., Hayakawa, K., Sato, T., & Imahori, K. (1973). Characterization and Genetic Analysis of a Mutant of *Escherichia coli* K-12 with Rounded Morphology. *Journal of Bacteriology*, *115*(1), 436–442.

Meeske, A. J., Riley, E. P., Robins, W. P., Uehara, T., Mekelanos, J. J., Kahne, D., Walker, S., Kruse, A. C., Bernhardt, T. G., & Rudner, D. Z. (2016). SEDS proteins are a widespread family of bacterial cell wall polymerases. *Nature*, *537*(7622), 634–638. https://doi.org/10.1038/nature19331

Megrian, D., Taib, N., Jaffe, A. L., Banfield, J. F., & Gribaldo, S. (2022). Ancient origin and constrained evolution of the division and cell wall gene cluster in Bacteria. *Nature Microbiology*, *7*(12), 2114–2127. https://doi.org/10.1038/s41564-022-01257-y

Minh, B. Q., Schmidt, H. A., Chernomor, O., Schrempf, D., Woodhams, M. D., von Haeseler, A., & Lanfear, R. (2020). IQ-TREE 2: New Models and Efficient Methods for Phylogenetic Inference in the Genomic Era. *Molecular Biology and Evolution*, *37*(5), 1530–1534. https://doi.org/10.1093/molbev/msaa015

Müh, U., Pannullo, A. G., Weiss, D. S., & Ellermeier, C. D. (2019). A Xylose-Inducible Expression System and a CRISPR Interference Plasmid for Targeted Knockdown of Gene Expression in *Clostridioides difficile*. *Journal of Bacteriology*, *201*(14). https://doi.org/10.1128/JB.00711-18

Murray, T., Popham, D. L., & Setlow, P. (1997). Identification and characterization of *pbpA* encoding *Bacillus subtilis* penicillin-binding protein 2A. *Journal of Bacteriology*, *179*(9), 3021–3029. https://doi.org/10.1128/jb.179.9.3021-3029.1997

Néron, B., Denise, R., Coluzzi, C., Touchon, M., Rocha, E. P. C., & Abby, S. S. (2023). MacSyFinder v2: Improved modelling and search engine to identify molecular systems in genomes. *Peer Community Journal*, *3*. https://doi.org/10.24072/pcjournal.250

Ng, Y. K., Ehsaan, M., Philip, S., Collery, M. M., Janoir, C., Collignon, A., Cartman, S. T., & Minton, N. P. (2013). Expanding the Repertoire of Gene Tools for Precise Manipulation of the *Clostridium difficile* Genome: Allelic Exchange Using *pyrE* Alleles. *PLOS ONE*, *8*(2), e56051. https://doi.org/10.1371/journal.pone.0056051

Nguyen, L.-T., Schmidt, H. A., von Haeseler, A., & Minh, B. Q. (2015). IQ-TREE: A Fast and Effective Stochastic Algorithm for Estimating Maximum-Likelihood Phylogenies. *Molecular Biology and Evolution*, *32*(1), 268–274. https://doi.org/10.1093/molbev/msu300

Nonejuie, P., Burkart, M., Pogliano, K., & Pogliano, J. (2013). Bacterial cytological profiling rapidly identifies the cellular pathways targeted by antibacterial molecules. *Proceedings of the National Academy of Sciences*, *110*(40), 16169–16174. https://doi.org/10.1073/pnas.1311066110

Oliveira, P. H., Ribis, J. W., Garrett, E. M., Trzilova, D., Kim, A., Sekulovic, O., Mead, E. A., Pak, T., Zhu, S., Deikus, G., Touchon, M., Lewis-Sandari, M., Beckford, C., Zeitouni, N. E., Altman, D. R., Webster, E., Oussenko, I., Bunyavanich, S., Aggarwal, A. K., … Fang, G. (2020). Epigenomic characterization of *Clostridioides difficile* finds a conserved DNA methyltransferase that mediates sporulation and pathogenesis. *Nature Microbiology*, *5*(1), Article 1. https://doi.org/10.1038/s41564-019-0613-4

Pazos, M., Peters, K., Boes, A., Safaei, Y., Kenward, C., Caveney, N. A., Laguri, C., Breukink, E., Strynadka, N. C. J., Simorre, J.-P., Terrak, M., & Vollmer, W. (2020). SPOR Proteins Are Required for Functionality of Class A Penicillin-Binding Proteins in Escherichia coli. *MBio*, *11*(6), e02796-20. https://doi.org/10.1128/mBio.02796-20

Perez, A. J., Cesbron, Y., Shaw, S. L., Bazan Villicana, J., Tsui, H.-C. T., Boersma, M. J., Ye, Z. A., Tovpeko, Y., Dekker, C., Holden, S., & Winkler, M. E. (2019). Movement dynamics of divisome proteins and PBP2x:FtsW in cells of *Streptococcus pneumoniae*. *Proceedings of the National Academy of Sciences*, *116*(8), 3211–3220. https://doi.org/10.1073/pnas.1816018116

Piggot, P. J., & Coote, J. G. (1976). Genetic aspects of bacterial endospore formation. *Microbiology and Molecular Biology Reviews*, *40*(4), 908–962.

Pinho, M. G., Filipe, S. R., de Lencastre, H., & Tomasz, A. (2001). Complementation of the Essential Peptidoglycan Transpeptidase Function of Penicillin-Binding Protein 2 (PBP2) by the Drug Resistance Protein PBP2A in *Staphylococcus aureus*. *Journal of Bacteriology*, *183*(22), 6525–6531. https://doi.org/10.1128/jb.183.22.6525-6531.2001

780 Pishdadian, K., Fimlaid, K. A., & Shen, A. (2015). SpoIIID-mediated regulation of σK function during
781 *Clostridium difficile* sporulation. *Molecular Microbiology*, *95*(2), 189–208.
782 https://doi.org/10.1111/mmi.12856
783 Pogliano, J., Osborne, N., Sharp, M. D., Abanes-De Mello, A., Perez, A., Sun, Y.-L., & Pogliano, K.
784 (1999). A vital stain for studying membrane dynamics in bacteria: A novel mechanism
785 controlling septation during Bacillus subtilis sporulation. *Molecular Microbiology*, *31*(4), 1149–
786 1159. https://doi.org/10.1046/j.1365-2958.1999.01255.x
787 Putnam, E. E., Nock, A. M., Lawley, T. D., & Shen, A. (2013). SpoIVA and SipL Are Clostridium
788 difficile Spore Morphogenetic Proteins. *Journal of Bacteriology*, *195*(6), 1214–1225.
789 https://doi.org/10.1128/jb.02181-12
790 Ransom, E. M., Weiss, D. S., & Ellermeier, C. D. (2016). Use of mCherryOpt Fluorescent Protein in
791 Clostridium difficile. In A. P. Roberts & P. Mullany (Eds.), *Clostridium difficile: Methods and*
792 *Protocols* (pp. 53–67). Springer. https://doi.org/10.1007/978-1-4939-6361-4_5
793 Ransom, E. M., Williams, K. B., Weiss, D. S., & Ellermeier, C. D. (2014). Identification and
794 characterization of a gene cluster required for proper rod shape, cell division, and pathogenesis in
795 *Clostridium difficile. Journal of Bacteriology*, *196*(12), 2290–2300.
796 https://doi.org/10.1128/JB.00038-14
797 Reichmann, N. T., Tavares, A. C., Saraiva, B. M., Jousselin, A., Reed, P., Pereira, A. R., Monteiro, J. M.,
798 Sobral, R. G., VanNieuwenhze, M. S., Fernandes, F., & Pinho, M. G. (2019). SEDS–bPBP pairs
799 direct lateral and septal peptidoglycan synthesis in *Staphylococcus aureus*. *Nature Microbiology*,
800 *4*(8), Article 8. https://doi.org/10.1038/s41564-019-0437-2
801 Rismondo, J., Halbedel, S., & Gründling, A. (2019). Cell Shape and Antibiotic Resistance Are
802 Maintained by the Activity of Multiple FtsW and RodA Enzymes in Listeria monocytogenes.
803 *mBio*, *10*(4), e01448-19. https://doi.org/10.1128/mBio.01448-19
804 Robichon, C., King, G. F., Goehring, N. W., & Beckwith, J. (2008). Artificial Septal Targeting of
805 Bacillus subtilis Cell Division Proteins in Escherichia coli: An Interspecies Approach to the
806 Study of Protein-Protein Interactions in Multiprotein Complexes. *Journal of Bacteriology*,
807 *190*(18), 6048–6059. https://doi.org/10.1128/JB.00462-08
808 Sacco, M. D., Wang, S., Adapa, S. R., Zhang, X., Gongora, M. V., Gatdula, J. R., Lewandowski, E. M.,
809 Hammond, L. R., Townsend, J. A., Marty, M. T., Wang, J., Eswara, P. J., Jiang, R. H. Y., Sun,
810 X., & Chen, Y. (2022). *A unique class of Zn2+-binding PBPs underlies cephalosporin resistance*
811 *and sporogenesis of Clostridioides difficile* (p. 2022.01.04.474981). bioRxiv.
812 https://doi.org/10.1101/2022.01.04.474981
813 Sassine, J., Xu, M., Sidiq, K. R., Emmins, R., Errington, J., & Daniel, R. A. (2017). Functional
814 redundancy of division specific penicillin-binding proteins in *Bacillus subtilis*. *Molecular*
815 *Microbiology*, *106*(2), 304–318. https://doi.org/10.1111/mmi.13765
816 Saujet, L., Pereira, F. C., Serrano, M., Soutourina, O., Monot, M., Shelyakin, P. V., Gelfand, M. S.,
817 Dupuy, B., Henriques, A. O., & Martin-Verstraete, I. (2013). Genome-Wide Analysis of Cell
818 Type-Specific Gene Transcription during Spore Formation in *Clostridium difficile*. *PLOS*
819 *Genetics*, *9*(10), e1003756. https://doi.org/10.1371/journal.pgen.1003756
820 Scheffers, D.-J., & Errington, J. (2004). PBP1 Is a Component of the *Bacillus subtilis* Cell Division
821 Machinery. *Journal of Bacteriology*, *186*(15), 5153–5156.
822 https://doi.org/10.1128/JB.186.15.5153-5156.2004
823 Schindelin, J., Arganda-Carreras, I., Frise, E., Kaynig, V., Longair, M., Pietzsch, T., Preibisch, S.,
824 Rueden, C., Saalfeld, S., Schmid, B., Tinevez, J.-Y., White, D. J., Hartenstein, V., Eliceiri, K.,
825 Tomancak, P., & Cardona, A. (2012). Fiji: An open-source platform for biological-image
826 analysis. *Nature Methods*, *9*(7), Article 7. https://doi.org/10.1038/nmeth.2019
827 Sher, J. W., Lim, H. C., & Bernhardt, T. G. (2021). Polar Growth in *Corynebacterium glutamicum* Has a
828 Flexible Cell Wall Synthase Requirement. *mBio*, e0068221. https://doi.org/10.1128/mBio.00682-
829 21

Sjodt, M., Rohs, P. D. A., Gilman, M. S. A., Erlandson, S. C., Zheng, S., Green, A. G., Brock, K. P., Taguchi, A., Kahne, D., Walker, S., Marks, D. S., Rudner, D. Z., Bernhardt, T. G., & Kruse, A. C. (2020). Structural coordination of polymerization and crosslinking by a SEDS–bPBP peptidoglycan synthase complex. *Nature Microbiology*, *5*(6), Article 6. https://doi.org/10.1038/s41564-020-0687-z

Spratt, B. G. (1975). Distinct penicillin binding proteins involved in the division, elongation, and shape of *Escherichia coli* K12. *Proceedings of the National Academy of Sciences*, *72*(8), 2999–3003. https://doi.org/10.1073/pnas.72.8.2999

Srikhanta, Y. N., Hutton, M. L., Awad, M. M., Drinkwater, N., Singleton, J., Day, S. L., Cunningham, B. A., McGowan, S., & Lyras, D. (2019). Cephamycins inhibit pathogen sporulation and effectively treat recurrent *Clostridioides difficile* infection. *Nature Microbiology*, *4*(12), 2237–2245. https://doi.org/10.1038/s41564-019-0519-1

Straume, D., Piechowiak, K. W., Kjos, M., & Håvarstein, L. S. (2021). Class A PBPs: It is time to rethink traditional paradigms. *Molecular Microbiology*, *116*(1), 41–52. https://doi.org/10.1111/mmi.14714

Straume, D., Piechowiak, K. W., Olsen, S., Stamsås, G. A., Berg, K. H., Kjos, M., Heggenhougen, M. V., Alcorlo, M., Hermoso, J. A., & Håvarstein, L. S. (2020). Class A PBPs have a distinct and unique role in the construction of the pneumococcal cell wall. *Proceedings of the National Academy of Sciences*, *117*(11), 6129–6138. https://doi.org/10.1073/pnas.1917820117

Stylianidou, S., Brennan, C., Nissen, S. B., Kuwada, N. J., & Wiggins, P. A. (2016). SuperSegger: Robust image segmentation, analysis and lineage tracking of bacterial cells. *Molecular Microbiology*, *102*(4), 690–700. https://doi.org/10.1111/mmi.13486

Taguchi, A., Welsh, M. A., Marmont, L. S., Lee, W., Sjodt, M., Kruse, A. C., Kahne, D., Bernhardt, T. G., & Walker, S. (2019). FtsW is a peptidoglycan polymerase that is functional only in complex with its cognate penicillin-binding protein. *Nature Microbiology*, *4*(4), Article 4. https://doi.org/10.1038/s41564-018-0345-x

Thompson, L. S., Beech, P. L., Real, G., Henriques, A. O., & Harry, E. J. (2006). Requirement for the cell division protein DivIB in polar cell division and engulfment during sporulation in *Bacillus subtilis*. *Journal of Bacteriology*, *188*(21), 7677–7685. https://doi.org/10.1128/JB.01072-06

Tsang, M.-J., & Bernhardt, T. G. (2015). A role for the FtsQLB complex in cytokinetic ring activation revealed by an *ftsL* allele that accelerates division. *Molecular Microbiology*, *95*(6), 925–944. https://doi.org/10.1111/mmi.12905

van den Belt, M., Gilchrist, C., Booth, T. J., Chooi, Y.-H., Medema, M. H., & Alanjary, M. (2023). CAGECAT: The CompArative GEne Cluster Analysis Toolbox for rapid search and visualisation of homologous gene clusters. *BMC Bioinformatics*, *24*(1), 181. https://doi.org/10.1186/s12859-023-05311-2

Vigouroux, A., Cordier, B., Aristov, A., Alvarez, L., Özbaykal, G., Chaze, T., Oldewurtel, E. R., Matondo, M., Cava, F., Bikard, D., & van Teeffelen, S. (2020). Class-A penicillin binding proteins do not contribute to cell shape but repair cell-wall defects. *ELife*, *9*, e51998. https://doi.org/10.7554/eLife.51998

Wacnik, K., Rao, V. A., Chen, X., Lafage, L., Pazos, M., Booth, S., Vollmer, W., Hobbs, J. K., Lewis, R. J., & Foster, S. J. (2022). Penicillin-Binding Protein 1 (PBP1) of *Staphylococcus aureus* Has Multiple Essential Functions in Cell Division. *mBio*, *13*(4), e00669-22. https://doi.org/10.1128/mbio.00669-22

Williams, M. A., Aliashkevich, A., Krol, E., Kuru, E., Bouchier, J. M., Rittichier, J., Brun, Y. V., VanNieuwenhze, M. S., Becker, A., Cava, F., & Brown, P. J. B. (2021). Unipolar Peptidoglycan Synthesis in the Rhizobiales Requires an Essential Class A Penicillin-Binding Protein. *mBio*, *12*(5), e02346-21. https://doi.org/10.1128/mBio.02346-21

Yanouri, A., Daniel, R. A., Errington, J., & Buchanan, C. E. (1993). Cloning and sequencing of the cell division gene pbpB, which encodes penicillin-binding protein 2B in *Bacillus subtilis*. *Journal of Bacteriology*, *175*(23), 7604–7616. https://doi.org/10.1128/jb.175.23.7604-7616.1993